

PREPARATION AND CHARACTERIZATION OF MAGNETITE  
NANOPARTICLES BY THERMAL DECOMPOSITION METHOD FOR  
THEIR POTENTIAL USE IN TUMOR IMAGING

A THESIS SUBMITTED TO  
THE GRADUATE SCHOOL OF NATURAL AND APPLIED SCIENCES  
OF  
MIDDLE EAST TECHNICAL UNIVERSITY

BY

ZEHRA TATLICI

IN PARTIAL FULFILLMENT OF THE REQUIREMENTS  
FOR  
THE DEGREE OF MASTER OF SCIENCE  
IN  
CHEMISTRY

DECEMBER 2010

Approval of the Thesis:

**PREPARATION AND CHARACTERIZATION OF SILICA COATED  
MAGNETITE NANOPARTICLES BY THERMAL DECOMPOSITION  
METHOD FOR THEIR POTENTIAL USE IN TUMOR IMAGING**

submitted by **ZEHRA TATLICI** in partial fulfillment of the requirements for the degree of **Master of Science in Chemistry Department, Middle East Technical University** by,

Prof. Dr. Canan Özgen  
Dean, Graduate School of **Natural and Applied Sciences** \_\_\_\_\_

Prof. Dr. İlker Özkan  
Head of Department, **Chemistry Department, METU** \_\_\_\_\_

Prof. Dr. Mürvet Volkan  
Supervisor, **Chemistry Department, METU** \_\_\_\_\_

**Examining Committee Members:**

Prof. Dr. O. Yavuz Ataman  
Chemistry Department, METU \_\_\_\_\_

Prof. Dr. Mürvet Volkan  
Chemistry Department, METU \_\_\_\_\_

Prof. Dr. Necati Özkan  
Polymer Science and Technology Department, METU \_\_\_\_\_

Prof. Dr. Raşit Turan  
Physics Department, METU \_\_\_\_\_

Prof. Dr. H. Ceyhan Kayran  
Chemistry Department, METU \_\_\_\_\_

Date: December 28, 2010

I hereby declare that all information in this document has been obtained and presented in accordance with academic rules and ethical conduct. I also declare that, as required by these rules and conduct, I have fully cited and referenced all material and results that are not original to this work.

Name, Last name : Zehra Tatlıcı

Signature :

## ABSTRACT

### **PREPARATION AND CHARACTERIZATION OF SILICA COATED MAGNETITE NANOPARTICLES BY THERMAL DECOMPOSITION METHOD FOR THEIR POTENTIAL USE IN TUMOR IMAGING**

Tatlıcı, Zehra

M.Sc., Department of Chemistry

Supervisor: Prof. Dr. Mürvet Volkan

December 2010, 75 pages

In biomedical applications, magnetic nanoparticles have been used as they offer attractive possibilities. First, they have controllable sizes ranging from a few nanometers up to tens of nanometers and second, the nanoparticles are magnetic and magnetic fields can penetrate into human tissue which means that they can be manipulated by an external magnetic field gradient. In this study,  $\text{Fe}_3\text{O}_4$  nanoparticles are synthesized by thermal decomposition method for their potential use in cancer diagnosis. Techniques like TEM, XRD, and FTIR were performed to control the properties of the synthesized particles whether they are suitable for certain applications. In thermal decomposition method, two different iron precursors were employed to obtain magnetite nanoparticles. In the usage of  $\text{Fe}(\text{acac})_3$ , approximate particle sizes obtained by this method lie between 3-6 nm. When,  $\text{Fe}(\text{CO})_5$  was used as the iron precursor, average particles size of 6 nm were obtained.

Rhenium carbonyl complex was prepared by reductive carboxylation utilizing gaseous carbon monoxide as a source of carbonyl and amino borane,  $\text{BH}_3\text{NH}_3$  as the

reducing agent. HPLC-ICP-MS was used for measuring complex formation. 95% conversion of perrhenate into the complex was seen. In this part, rhenium is selected as a surrogate of radioactive  $^{99m}\text{Tc}$ .  $^{188}\text{Re}$  and  $^{186}\text{Re}$  can also be used in radioactive therapy.

Keywords: Magnetite nanoparticles, silica coating, thermal decomposition method, Tc-99m, radioactive therapy

## ÖZ

# POTANSİYEL TÜMÖR GÖRÜNTÜLEMEDE KULLANILMAK AMACI İLE MAGNETİT NANOPARÇACIKLARIN TERMAL PARÇALANMA YÖNTEMİ İLE HAZIRLANMASI

Tatlıcı, Zehra

Yüksek Lisans, Kimya Bölümü

Tez Yöneticisi: Prof. Dr. Mürvet Volkan

Aralık 2010, 75 sayfa

Manyetik nanoparçacıklar, sağladıkları cazip imkanlar nedeniyle biyomedikal uygulamalarda sıkça kullanılmaktadırlar. İlk olarak, birkaç nanometreden onlarca nanometreye kadar değişen kontrol edilebilir boyutlara sahiptirler. Ayrıca, nanoparçacıklar manyetik özelliğe sahiptir ve manyetik alan insan dokusunun içine sızabilir, yani insan dokusu içinde dış bir manyetik alan etkisiyle işlem yapılabilir. Bu çalışmada,  $Fe_3O_4$  nanoparçacıklar, tümör tanımlama için potansiyel kullanımları nedeniyle, yüksek sıcaklıkla parçalanma yoluyla sentezlenmiştir.

Belirli kullanımlar için uygun olup olmadığını test etmek amacıyla, sentezlenen parçacıkların özellikleri TEM, XRD ve FTIR gibi teknikler kullanılarak kontrol edilmiştir. Yüksek sıcaklıkla parçalanma metodunda, manyetik nanoparçacık eldesi için iki farklı demir öncü maddesi denenmiştir. Demir asetil asetonat'ın öncü madde olarak kullanıldığı çalışmalarda, parçacık boyutları 3 nm ile 6 nm arasında değişmektedir. Demir pentakarbonil'in öncü madde olarak kullanıldığı çalışmada ise ortalama parçacık boyutu 6 nm civarındadır.

Renyum karbonil kompleksi indirgeyici karboksilasyon yoluyla hazırlanmış, karbonil ve aminoboran kaynağı olarak gaz durumundaki karbonmonoksit, indirgen madde olarak ise,  $\text{BH}_3\text{NH}_3$  kullanılmıştır. Kompleks oluşumunu ölçmek amacıyla Yüksek Performanslı Sıvı Kromatografi – İndüktif Eşleşmiş Plazma Kütle Spektrometresi kullanılmış ve perrenat'ın %95'inin komplekse dönüştüğü görülmüştür. Bu çalışmada  $^{99\text{m}}\text{Tc}$ 'in vekili olarak kullanılan Renyum, diğer çalışmalarda radyoaktif izotoplar olan  $^{188}\text{Re}$  ve  $^{186}\text{Re}$  seçilerek, radyoaktif terapide de kullanılabilir.

Anahtar Kelimeler: Magnetit nanoparçacıklar, silika kaplama, yüksek sıcaklıkta parçalanma metodu, Tc-99m, radyoaktif terapi

To My Father,  
*Wish you were here*

## ACKNOWLEDGEMENTS

I would like to express my special thanks to my supervisor Prof. Dr. Mürvet Volkan for her valuable guidance, support, encouragement and patience.

I would like to thank Prof. Dr. Necati Özkan for his guidance.

I would like to thank Murat Kaya nothing special but everything he made during my study.

I am so pleased to meet Dr. Elif Tarhan Bor during this study. Not only she helped me so much during TEM measurements in Central Laboratory but also she gave me moral support and warm friendship. Thank her so much for everything.

I would like to thank Dr. Sezgin Bakırdere for his guidance and support.

I am deeply grateful to my team mate Ümit Zengin for his cooperation, help and friendship.

Special thanks to Mervegül Maden, Bahar Köksel, Zeynep Ergül and Gülfem Aygar for their love and encouragement. They believe and support me all the times. They are very valuable gifts to my following life from this study.

I would like to thank Tuba Nur Aslan, Tacettin Öztürk, Ufuk Özgen for their help, ideas and friendship and all C50 and C49 lab members.

Endless thanks to my dear mother, Hatice Tatlıcı for her assets, love, trust and patience. She gave me endless love, believe me and support me in every situation.

Great thanks to S. Seda Güney, Alev Güney and Uğur Güney for their endless love and support. No matter how far we were, they were always with me.

Special thanks to Güzden Varinlioğlu and Emrah Cantekin for their friendship. Whenever I laugh and whenever I cry, they were always with me.

Huge thanks to Ekin Tuncalı, A. Damla Atalay, Belek Öztürkcan, Evren Koban, Fulya Levent, Burçe Çiftçi, Esra Demirkol, Fatoş Alp, Meliz Mertay and Burak

Özkırlı for their friendship, love and support. I am very lucky to have such good friends, whenever I need them, they were always with me.

I would like to thank Eczacıbaşı Monrol Nuclear Products and Turkish Republic Ministry of Industry and Trade for supplying financial support during my master work.

## TABLE OF CONTENT

ABSTRACT .....	iv
ÖZ .....	vi
ACKNOWLEDGEMENTS .....	ix
Table of Contents .....	xi
List of Figures .....	xiv
List of Tables .....	xviii
LIST OF ABBREVIATIONS .....	xix
CHAPTERS	
1. INTRODUCTION .....	1
1.1 Nanomaterials .....	1
1.2 Magnetism and Magnetic Properties .....	2
1.2.1 Diamagnetism .....	3
1.2.2 Paramagnetism .....	4
1.2.3 Ferromagnetism .....	4
1.2.4 Antiferromagnetism .....	5
1.2.5 Superparamagnetism .....	6
1.3 Magnetic Iron Oxide Nanoparticles .....	7
1.3.1 Magnetite .....	8
1.4 Applications of Magnetic Nanoparticles .....	9
1.5 Synthesis of Magnetic Nanoparticles .....	11
1.5.1 Microemulsions .....	11
1.5.2 Spray Pyrolysis .....	11
1.5.3 Polyols .....	12
1.5.4 Coprecipitation .....	12
1.5.5 Thermal Decomposition Method .....	12
1.6 Nuclear Medicine and Imaging .....	13
1.7 Radiation Chemistry .....	14
1.8 Imaging Agents .....	16
1.8.1 Technetium .....	16
1.8.2 Rhenium .....	17

1.9	Aim of this study .....	19
2.	EXPERIMENTAL.....	20
2.1	Synthesis of Iron Nanoparticles by Thermal Decomposition Method 1 .	20
2.1.1	Chemicals and Reagents.....	20
ii.	1,2 Hexadecanediol, technical grade .....	20
2.1.2	Procedure.....	21
2.2	Synthesis of Iron Nanoparticles by Thermal Decomposition Method 2 .	23
2.2.1	Chemicals and Reagent .....	23
2.2.2	Procedure.....	23
2.3	Synthesis of $[\text{Re}(\text{CO})_3(\text{OH}_2)_3]^+$ Complex.....	25
2.3.1	Chemicals and Reagent .....	25
2.3.2	Procedure.....	26
2.4	Instruments Used in Characterization Studies.....	28
2.4.1	Centrifuge.....	28
2.4.2	Field Emission Scanning Electron Microscopy (FE-SEM) .....	28
2.4.3	Transmission Electron Microscopy (TEM).....	28
2.4.4	Fourier Transform Infrared Spectroscopy (FTIR).....	29
2.4.5	Energy Dispersive X-Ray Spectroscopy (EDX) .....	29
2.4.6	X-Ray Diffraction (XRD).....	29
2.4.7	High-Performance Liquid Chromatography- Inductively Coupled Plasma- Mass Spectrometer (HPLC- ICP- MS).....	30
2.5	Structures of Chemical Compounds Used in Procedures .....	32
3.	RESULTS AND DISCUSSION .....	34
3.1	Synthesis of Iron Oxide Nanoparticles by Thermal Decomposition Method.....	34
3.1.1	Effect of Iron Precursor on Nanoparticle Formation.....	37
3.1.2	The Effect of Reaction Temperature (solvent boiling point) on Nanoparticle Formation .....	40
3.1.3	The Effect of Reflux Time on Particle Formation.....	48
3.1.4	Effect of Iron Precursor to Oleic Acid Ratio.....	51
3.1.5	IR Studies .....	56
3.1.6	Magnetic Properties of Synthesized Magnetite Nanoparticles.....	57
3.1.7	XRD Measurements of the Iron Oxide Nanoparticles .....	58

3.2	Synthesis of Re Carbonyl Complex.....	62
3.2.1	Optimization Studies .....	64
4.	CONCLUSION .....	69
	REFERENCES.....	71

## LIST OF FIGURES

Figure 1. Biological materials and their size comparison on nanoscale .....	2
Figure 2 Orientation of diamagnetic materials.....	3
Figure 3 Orientation of Paramagnetic Materials.....	4
Figure 4. Orientation of Ferromagnetic Materials .....	5
Figure 5. Orientation of Antiferromagnetic Materials .....	5
Figure 6 Magnetization curve on H/T bases as a demonstration of superparamagnetism.....	7
Figure 7 Structure of magnetite .....	8
Figure 8 Applications of magnetic nanoparticles.....	9
Figure 9 Experimental setup for synthesis of magnetic nanoparticles with Thermal Decomposition Method.....	22
Figure 10 a.Initial orange color of the solution. b. Smoke can be seen. c. Final black color of the solution.....	25
Figure 11. Formation of Re carbonyl complex .....	26
Figure 12 a. Filling of vial with CO for 20 min. b. Experimental setup for complex synthesis c. Radiolabeling by adding Re- perrhenate into the vial and incubated in water bath at 70-80° .....	27
Figure 13 TEM image of magnetite nanoparticles synthesized by thermal decomposition method. Iron precursor = Fe(acac) <sub>3</sub> , solvent = phenyl ether, reflux time < 30 minutes, Fe(acac) <sub>3</sub> : oleic acid = 1:3 .....	36
Figure 14 TEM image of magnetite nanoparticles synthesized by thermal decomposition method. Iron precursor = Fe(acac) <sub>3</sub> , solvent = phenyl ether, reflux time = 30 minutes, Fe(acac) <sub>3</sub> : oleic acid = 1:3 .....	37
Figure 15 TEM image of magnetite nanoparticles synthesized by thermal decomposition method. Iron precursor= Fe(acac) <sub>3</sub> , solvent= phenyl ether, reflux time= 30 minutes, Fe(acac) <sub>3</sub> : oleic acid= 1:3, N=25, average particle size= 5.55 nm, standard deviation= 0.71 .....	38
Figure 16 TEM image of magnetite nanoparticles synthesized by thermal decomposition method. Iron precursor= Fe(CO) <sub>5</sub> , solvent= benzyl ether, reflux time=	

60 minutes, Fe(CO) <sub>5</sub> : oleic acid= 1:3, N= 15, average particle size= 8.86 nm, standard deviation= 2.91 .....	39
Figure 17 TEM image of magnetite nanoparticles synthesized by thermal decomposition method. Iron precursor= Fe(CO) <sub>5</sub> , solvent= benzyl ether, reflux time= 60 minutes, Fe(CO) <sub>5</sub> : oleic acid= 1:3, N= 12, average particle size= 8.86 nm, standard deviation= 2.91 .....	41
Figure 18 Particle size versus number of particles diagram of nanoparticles in Figure 17.....	41
Figure 19 TEM image of magnetite nanoparticles synthesized by thermal decomposition method. Iron precursor= Fe(acac) <sub>3</sub> , solvent = benzyl ether, reflux time= 30 minutes, Fe(acac) <sub>3</sub> : oleic acid= 1:3, N= 25, average particle size= 5.62 nm, standard deviation= 0.54 .....	42
Figure 20 Particle size versus number of particles diagram of particles in Figure 19... ..	42
Figure 21 TEM image of magnetite nanoparticles synthesized by thermal decomposition method. Iron precursor= Fe(acac) <sub>3</sub> , solvent= benzyl ether, reflux time= 30 minutes, Fe(acac) <sub>3</sub> : oleic acid= 1:3, N=25, average particle size= 6.53 nm, standard deviation= 1.03 .....	43
Figure 22 Particle size versus number of particles diagram of particles in Figure 21	43
Figure 23 TEM image of magnetite nanoparticles synthesized by thermal decomposition method. Iron precursor= Fe(CO) <sub>5</sub> , solvent = phenyl ether, reflux time= 60 minutes, Fe(CO) <sub>5</sub> : oleic acid= 1:3, N=25, average particle size= 7.40 nm, standard deviation= 2.21 .....	44
Figure 24 Particle size versus number of particles graph of particles in Figure 23 ...	44
Figure 25 TEM image of magnetite nanoparticles synthesized by thermal decomposition method. Iron precursor= Fe(acac) <sub>3</sub> , solvent = phenyl ether, reflux time = 30 minutes, Fe(acac) <sub>3</sub> : oleic acid = 1:3, N=25, average particle size = 7.65 nm, standard deviation= 1.23 .....	45
Figure 26 Particle size versus number percent graph of Figure 25.....	45
Figure 27 TEM image of magnetite nanoparticles synthesized by thermal decomposition method. Iron precursor= Fe(acac) <sub>5</sub> , solvent = phenyl ether, reflux	

time = 30 minutes, Fe(acac) <sub>3</sub> : oleic acid = 1:3, N=25, average particle size = 7.97 nm, standard deviation= 1.44 .....	46
Figure 28 Particle size versus percent number of particles in Figure 27 .....	47
Figure 29 TEM image of magnetite nanoparticles synthesized thermal decomposition method. Iron precursor= Fe(acac) <sub>3</sub> , solvent = phenyl ether, reflux time < 30 minutes, Fe(acac) <sub>3</sub> : oleic acid = 1:3 .....	48
Figure 30. TEM image of magnetite nanoparticles synthesized by thermal decomposition method. Iron precursor= Fe(acac) <sub>3</sub> , solvent = phenyl ether, reflux time = 0 minutes, Fe(acac) <sub>3</sub> : oleic acid = 1:3 .....	49
Figure 31 TEM image of magnetite nanoparticles synthesized by thermal decomposition method. Iron precursor = Fe(acac) <sub>3</sub> , solvent = benzyl ether, reflux time = 60 minutes, Fe(acac) <sub>3</sub> : oleic acid = 1:3 .....	50
Figure 32. TEM image of magnetite nanoparticles synthesized by thermal decomposition method. Iron precursor = Fe(acac) <sub>3</sub> , solvent = benzyl ether, reflux time = 30 minutes, Fe(acac) <sub>3</sub> : oleic acid = 1:1, N=25, average particle size = 4.03 nm, standard deviation= 0.69 .....	51
Figure 33 Particle size versus percent number graph of Figure 30.....	52
Figure 34. TEM image of magnetite nanoparticles synthesized by thermal decomposition method. Iron precursor = Fe(acac) <sub>3</sub> , solvent = benzyl ether, reflux time = 30 minutes, Fe(acac) <sub>3</sub> : oleic acid = 1:3, N=25, average particle size = 5.55 nm, standard deviation= 0.71 .....	52
Figure 35 Particle size versus percent number diagram of Figure 31.....	53
Figure 36. TEM image of magnetite nanoparticles synthesized by thermal decomposition method. Iron precursor = Fe(acac) <sub>3</sub> , solvent = benzyl ether, reflux time = 30 minutes, Fe(acac) <sub>3</sub> : oleic acid = 1:5, N=50, average particle size = 6.52 nm, standard deviation= 0.92 .....	54
Figure 37 Particle size versus number of particles diagram of Figure 33.....	54
Figure 38 Particle size distribution curve of magnetite nanoparticles that is synthesized by Fe(acac) <sub>3</sub> and benzyl ether.....	55
Figure 39 FT-IR spectrum of Fe <sub>3</sub> O <sub>4</sub> nanoparticles.....	56
Figure 40 Pictures of magnetite nanoparticles after 5 minute, 30 minute, 1 hour and 2 hours after the synthesis .....	57

Figure 41 X- Ray Diffraction pattern of two week magnetite nanoparticles prepared by phenyl ether and Fe(acac) <sub>3</sub> .....	58
Figure 42 X- Ray Diffraction pattern of two weeks magnetite prepared by benzyl ether and Fe(acac) <sub>3</sub> .....	60
Figure 43. Metal Tricarbonyl formation by reductive carboxylation .....	62
Figure 44 Optimization studies using Cation Exchange Column .....	65
Figure 45 Optimization studies using Anion Exchange Column.....	66
Figure 46 HPLC-ICP-MS, anion echange column chromatogram of rhenium carbonyl complex with optimal conditions.....	67
Figure 47 Complex formation yields at different CO gas flushing times .....	68

## LIST OF TABLES

Table 1 Radioactive Isotope Commonly Used as Sources of Radiation.....	15
Table 2 Isotopes of Technetium.....	17
Table 3 Radioactive Isotopes of Rhenium .....	18
Table 4 Structures of compounds used in experiments.....	32
Table 5 Theoretical (ICDD Card No: 75-1610) and measured crystal parameters of two weeks magnetite nanoparticles.....	59
Table 6 Theoretical (ICDD Card No: 75-1610) and measured crystal parameters of two weeks magnetite nanoparticles.....	61

## LIST OF ABBREVIATIONS

B	Magnetic Induction
EDX	Energy Dispersive X-ray Spectrometry
FE-SEM	Field Emission Scanning Electron Microscopy
FT-IR	Fourier Transform Infrared Spectroscopy
H	Magnetic Field
HPLC-ICP-MS	High Performance Liquid Chromatography- Inductively Coupled Plasma Mass Spectrometry
M	Magnetization
MRI	Magnetic Resonance Imaging
$M_s$	Saturation Magnetisation
TEM	Transmission Electron Microscopy
XRD	X- Ray Diffractometry
$\chi$	susceptibility
$\mu$	permeability
$\tau$	relaxation time

## CHAPTER 1

### INTRODUCTION

#### 1.1 Nanomaterials

“Nano”, meaning dwarf in Greek, is the SI prefix meaning  $10^{-9}$  of a unit. It is equal to one billionth ( $10^{-9}$ ) of a meter (Varadan, Chen, & Xie, 2008)

Considerable number of biological entities such as proteins, antibodies, viruses and bacteria are in the range of size smaller than 100 nm. They are usually called “biological nanomaterials” (Yih & Wei, 2005)

Nanoparticles that are smaller than 50 nm can penetrate in most of the cells and the ones that are smaller than 20 nm can travel within the circulatory system of the body and move out of the blood vessels.

Nanomaterials are important because of two reasons. First, they have larger surface area compared to materials with same mass but larger form. Larger area gives them reactivity and affect mechanical and optical properties of the materials. Second, nanomaterials are very suitable places for “quantum effects”. “Quantum effects” can change the material’s optical, magnetic and electrical properties and dominate the behaviors of a material at nanoscale.

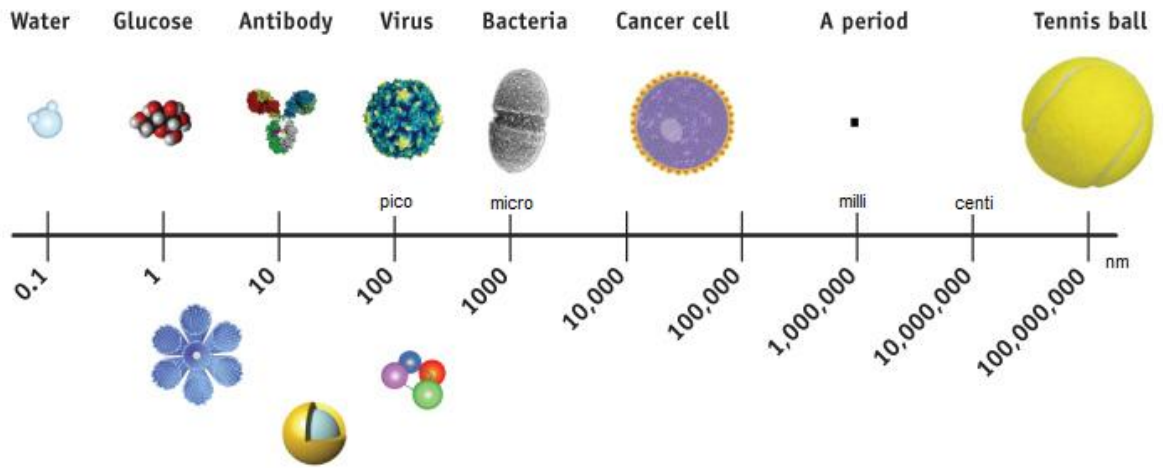


**Figure 1. Biological materials and their size comparison on nanoscale**

## 1.2 Magnetism and Magnetic Properties

When a magnetic field,  $H$  is applied to a material, it responds  $B$ , which is called its magnetic inductions. The relationship between  $B$  and  $H$  is a property of the material. The equation relating  $B$  and  $H$  is:

$$B = H + 4\pi M$$

$M$ , the magnetization of the medium, is the magnetic dipole moment per unit volume of material,

$$M = m / V \text{ ( emu/ cm}^3 \text{ )}$$

$M$  is a property of the material, and depends on both the individual magnetic moments of the constituent ions, atoms and molecules, and on how these dipole moments interact with each other (Spaldin, 2003).

“Spontaneous magnetization”  $M_s$  values of the ferromagnetic elements Fe, Co and Ni at 296 K are 1720, 1370 and 485 kA m<sup>-1</sup> respectively. Fe<sub>3</sub>O<sub>4</sub>, magnetite has  $M_s$  value of 480 kA m<sup>-1</sup> (Coey, 2010).

The properties of a material are defined not only by the magnetization, or the magnetic induction, but also by the way in which these quantities vary with the applied magnetic field.

$$X = M / H \text{ (emu/ cm}^3 \text{ Oe)}$$

The susceptibility indicates the responsiveness of a material to an applied magnetic field.

The ratio of B to H is called the permeability

$$\mu = B / H \text{ ( gauss/ Oe)}$$

and  $\mu$  indicates how permeable the material is to the magnetic field (Spaldin, 2003).

### 1.2.1 Diamagnetism

Diamagnetism is a very weak form of magnetism. It results from changes in electron orbital motion that are induced by an external field. Diamagnetism leads to a very weak magnetization which opposes the applied field. Copper, Gold, Bismuth, Silver, Helium, all the noble gases and hydrogen molecule are diamagnetic (Jiles, 1998) (Coey, 2010).

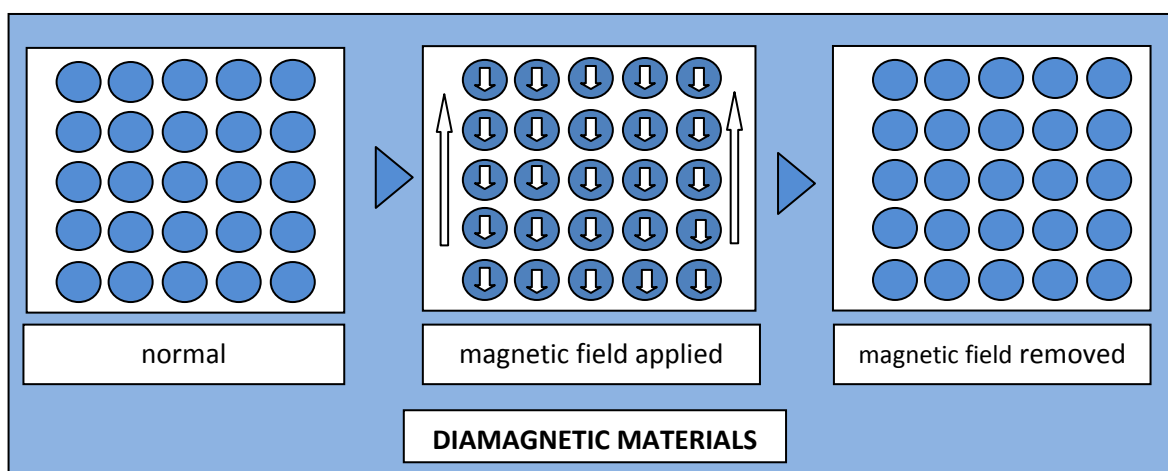


**Figure 2 Orientation of diamagnetic materials**

### 1.2.2 Paramagnetism

Paramagnetic materials are those that normally do not possess permanent magnetization but possess magnetization only in the presence of an external magnetic field. Aluminum and oxygen molecule are paramagnetic. All ferromagnetic materials become paramagnetic above their Neel temperature (Jiles, 1998).

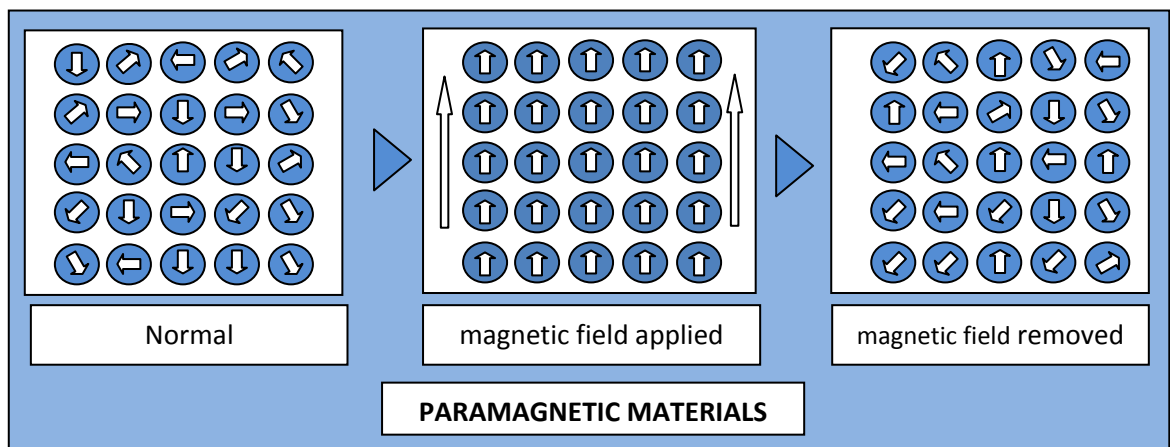


**Figure 3 Orientation of Paramagnetic Materials**

### 1.2.3 Ferromagnetism

Some metallic materials show very large and permanent magnetic moment even in the absence of an external field. When all the magnetic dipoles are aligned parallel with the external field, ferromagnetic materials possess their maximum possible magnetization. The possible magnetization is the saturation magnetization of materials. The saturation magnetization is maximum at 0 K, at that temperature the thermal vibrations are minimum. When temperature is increased, the saturation magnetization reduces and then drops to zero at what is called the “Curie temperature”,  $T_c$ . Above  $T_c$ , ferromagnetic materials are paramagnetic (Coey, 2010) (Jiles, 1998).



**Figure 4. Orientation of Ferromagnetic Materials**

#### 1.2.4 Antiferromagnetism

In antiferromagnetic materials, the magnetic dipole moments tends to align antiparallel to each other. Antiferromagnets have no net spontaneous magnetization. Antiferromagnetism is also affected by temperature. Néel temperature is the point above which antiferromagnetic materials become paramagnetic. Manganese oxide (MnO) is antiferromagnetic (Coey, 2010) (Jiles, 1998).

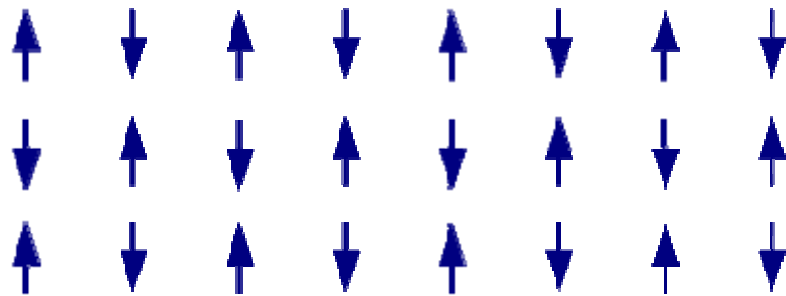


**Figure 5. Orientation of Antiferromagnetic Materials**

### 1.2.5 Superparamagnetism

Neel (1949) theoretically showed that as the thermal fluctuations of very small particles can prevent the existence of a stable magnetization,  $H_c$  approaches zero when particle becomes very small. Superparamagnetism has two experimental criteria (Bean & Jacob, 1956). First, there is no hysteresis for magnetization curve for supermagnetism. Second, superposing in a plot of  $M$  vs  $H/T$  of the magnetization curves at different temperatures for superparamagnetism (Varadan, Chen, & Xie, 2008).

Basic mechanism of superparamagnetism is related with the relaxation time  $\tau$  of the net magnetization of magnetic particle (Brown, 1963).

$$\tau = \tau_0 \exp \frac{\Delta E}{k_B T}$$

where  $\Delta E$  is the energy barrier to moment reversal,  $k_B T$  is the thermal energy.

For non- interacting particles the pre- exponential factor  $\tau_0$  is in the order of  $10^{-10}$ - $10^{-12}$  and depend weakly on temperature (Pankhurst, Connolly, Jones, & Dobson, 2003).

It is given by  $\Delta E = KV$ , where  $K$  is the anisotropy energy density and  $V$  is the particle volume. For small particles,  $\Delta E$  is comparable to  $k_B T$  at room temperature, so superparamagnetism is important for small particles.

Observations showed that in a given material, superparamagnetism is dependent on two parameters. These are the temperature and the measurement time  $\tau_m$  of the experimental technique used (Pankhurst, Connolly, Jones, & Dobson, 2003).

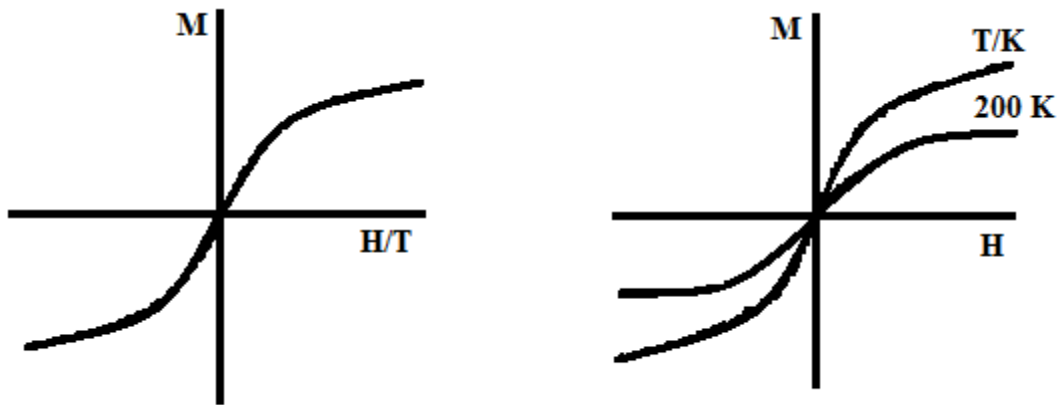


**Figure 6 Magnetization curve on H/T bases as a demonstration of superparamagnetism**

### 1.3 Magnetic Iron Oxide Nanoparticles

Properties like superparamagnetism, high coercivity, low Curie temperature and high magnetic susceptibility give iron oxide nanoparticles a great importance. They are used in broad range of area such as magnetic fluids, data storage and catalysis to bioactivations. Choice of the nanomaterial with suitable physical and chemical properties plays an important role in these applications (Wu, He, & Jiang, 2008).

Magnetic nanoparticles offer great advantages in biomedicine. First, they have variable size that is changed between a few to tens of nanometers. As they are small, they can enter a biological unit. When they are coated with a suitable biological molecule, they can interact with or bind to a biological unit, giving a controlled means of tagging (Pankhurst, Connolly, Jones, & Dobson, 2003). Second, by using an external magnetic field, magnetic nanoparticles can be controlled. With the help of this property, magnetic nanoparticles can be moved externally to a specific area and tag biological units magnetically (Varadan, Chen, & Xie, 2008).

### 1.3.1 Magnetite

Magnetite is a black mineral which exhibits the strongest magnetism among the transition metal oxides (Teja & Koh, 2009).

Magnetite has a cubic inverse spinel structure as shown in Figure 7. In this structure, oxygen anions form a FCC closed packing and Fe cations occupy the interstitial tetrahedral sites and octahedral sites. The electrons can travel between  $\text{Fe}^{2+}$  and  $\text{Fe}^{3+}$  ions in the octahedral sites at room temperature giving magnetite an important character of half-metallic materials (Xu, et al., 2007). The difference of maghemite from magnetite is that, all or most of the Fe in maghemite is in  $\text{Fe}^{3+}$  state.

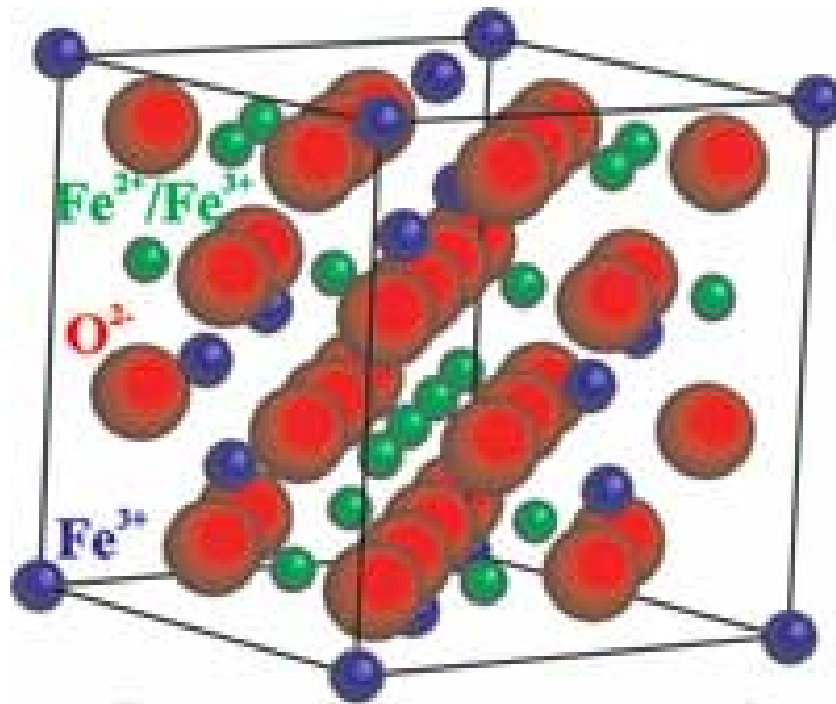


Figure 7 Structure of magnetite

## 1.4 Applications of Magnetic Nanoparticles

Magnetic nanoparticles with different forms and sizes have a lot of applications. Some applications of magnetic nanoparticles in biomedicine is shown in Figure 8.

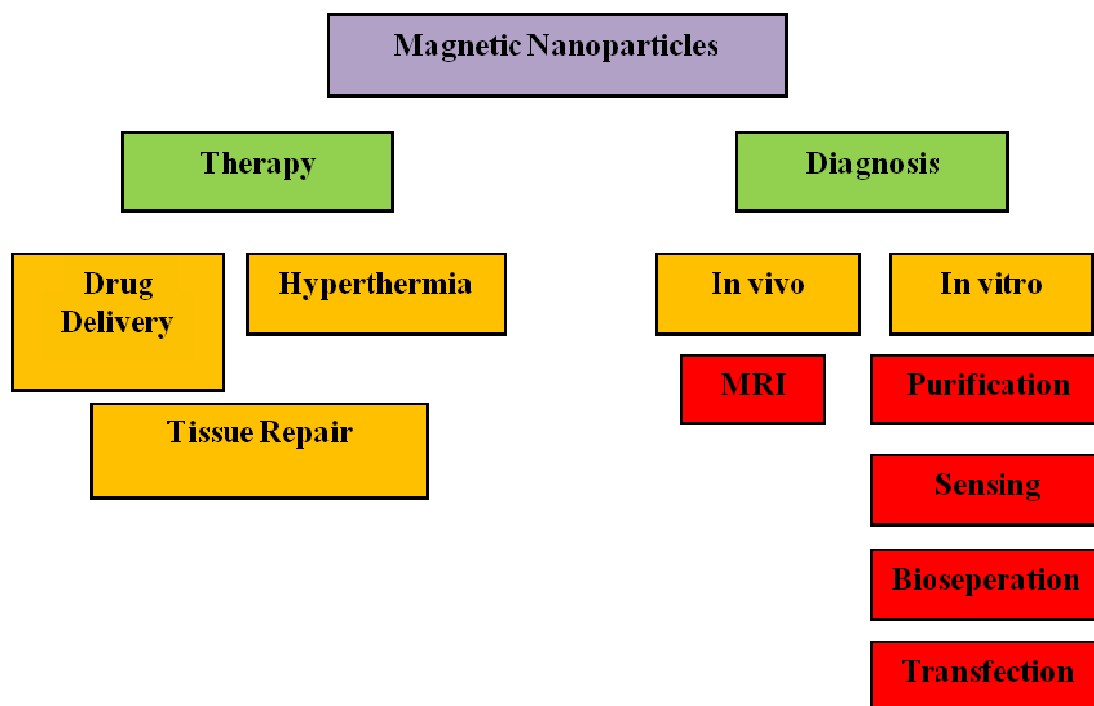


Figure 8 Applications of magnetic nanoparticles

“**Drug delivery**” is an important application of magnetic nanoparticles. Magnetic nanoparticles are used in delivery of drugs to specific site. In such applications, the charge, surface chemistry and size of the magnetic particles affect both the blood circulation time and bio availability of the particles within the body (Chouly, Pouliquen, Lucet, Jeune, & Pellet, 1996). Also, magnetic properties and internalization of the particles also depends on particle size. Particles with size of 10 to 100 nm are suitable for intravenous injection, the particles with these sizes can penetrate into the very small capillaries within the body tissues without being distinguished by reticuloendothelial system (RES) of the body (Pratsinis & Vemury, 1996). In magnetic targeting, a drug or therapeutic radioisotope is bound to a

magnetic compound, injected into blood stream and then stopped with a powerful magnetic field in the target area (Hafeli U. , 2004).

**“Hyperthermia”** is a process in which heat is used in the treatment of malignant tumours. Magnetic hysteresis loss causes generation of heat when magnetic particles are exposed to variable magnetic field. The magnetic properties of the material, the strength of the magnetic field, the frequency of oscillation and the cooling capacity of the blood flow in the tumour site affect the amount of heat generated (Gupta & Gupta, 2005). Temperatures higher than 42-43° C is needed for destruction of cancer cells whereas healthy cells can survive at that temperatures (Tartaj, Morales, Verdaguer, Carreno, & Serna, 2003).

**“Tissue repair”** using iron oxide nanoparticles is done through welding or soldering. In welding, two tissue surfaces are put side by side and heated sufficiently to join them. In soldering, nanoparticles that is coated with protein were placed between two tissue surfaces to join them. For both procedures, temperatures greater than 50°C is needed (Lobel, Eyal, Kariv, & Katzir, 1999). After denaturation of proteins and entanglement of adjacent protein chains, tissues were joined. Light absorbing nanoparticles are useful for tissue-repairing procedures (Xu, Smith, & Simon, 2004). They are coated onto the surface of two pieces of tissues for which joining was desired and least harmful wavelength of light and/or lower powered light sources are used.

To differentiate healthy tissues from pathological ones, superparamagnetic iron oxide nanoparticles play an important role as a **“Magnetic Resonance Imaging (MRI)”** contrast agents. Cell should be tag magnetically in order to visualize and track cells by MR Imaging. The MRI is used to diagnose disease, make pre-surgical assessment and monitor the effects of therapy. A lot of study is performed to increase contrast and

resolution of MRI. Magnetic nanoparticles coated with a material that is bioconjugate with the body is used as contrast agent (Varadan, Chen, & Xie, 2008).

## **1.5 Synthesis of Magnetic Nanoparticles**

In almost all applications, the particle size, shape, the size distribution, the surface chemistry of the particles and their magnetic properties are very important. Some of the methods used for synthesizing nanoparticles are described below.

### **1.5.1 Microemulsions**

Water-in-oil microemulsions the one of the simplest method for synthesizing magnetic nanoparticles. They are transparent, isotropic, thermodynamically stable liquid media. In microemulsions, aqueous phase is surrounded by surfactant molecules that are dispersed in oil phase. By the confinement effect of these surfactant-stabilized microcavities, particle nucleation, growth and agglomeration are limited (Pileni, 1993).

### **1.5.2 Spray Pyrolysis**

Spray pyrolysis is a process in which nanoparticles are deposited on a heated surface by spraying a solution into a series of reactors where aerosol droplets undergo evaporation of the solvent and condensation of the solute within the droplet. The reactants are selected such that the products other than the desired compound are volatile at the temperature of deposition (Messing, Zhang, & Jayanthi, 1993).

### **1.5.3 Polyols**

Polyol is a method by which uniform nanoparticles can be obtained. By this method metal particles such as copper, nickel and iron nanoparticles can be obtained by reduction of metal salt and direct metal precipitation from a solution containing a high boiling solvent, polyol such as diethylene glycol and ethylene glycol. In this method, the polyol act as the high boiling solvent of the metallic precursor, the reducing agent (Matijevic, 1993) as well as the stabilizer that control the growth of the particles and prevent interparticle aggregating (Cai & Wan, 2007).

### **1.5.4 Coprecipitation**

Coprecipitation is the most common method for production of magnetic nanoparticles in which coprecipitation of ferrous and ferric salts in an alkaline medium takes place. The mean particle size of nanoparticle is dependent on pH and the ionic strength of the precipitation medium. They are inversely proportional with the size of nanoparticles obtained. Both of these parameters affect the chemical composition of the surface and consequently, the electrostatic surface charge of the particles (Jolivet, 2000).

### **1.5.5 Thermal Decomposition Method**

In synthesis of magnetic nanoparticles, this method is the one of the most common methods to produce magnetite nanoparticles with good size control, narrow size distribution and excellent crystallinity of individual nanoparticles (Roca, Marco, Morales, & Serna, 2007) with the ability of self assembly (Simeonidis, et al., 2007). Many biomedical applications like magnetic resonance imaging, magnetic cell separation and magneto relaxometry depend on particle size and thus this method is potentially used for these applications.

In this method, iron compounds with oxygen-containing ligands such as acetylacetonates, acetates or oleates are decomposed at high temperature in surfactant containing solutions (Bronstein, et al., 2007). When iron precursor is added into a heated solution in the presence of surfactant, nucleation occurs and at higher temperatures, the growth stage took place (Simeonidis, et al., 2007). The narrow particle size distribution is due to the separation on the temperature scale of nucleation and growth processes. Shapes, sizes and crystal structures of formed nanoparticles depend on the reaction time, the reaction temperature (solvent boiling point) and Fe/surfactant molar ratio. Saturated hydrocarbons of different length are used as solvents because they provide a variety of boiling points and they are more chemically inert at high temperatures than many other solvents (Bronstein, et al., 2007) (Caruntu, Caruntu, Chen, O'Connor, Goloverda, & Kolesnşchenko, 2004).

## **1.6 Nuclear Medicine and Imaging**

Cancer is the most dangerous threat to human health. Chemotherapy, radiotherapy and surgery are currently used for cancer treatment (Chunfu, Jinquan, Duanzhi, Yongxian, Yanlin, & Jiajü, 2004). Treatment is effective when it kills the cancer cells while giving as fewer damage to healthy cells as possible (Liang, Wang, Yu, Zhang, Xia, & Yin, 2007).

In nuclear medicine, two different types of radiotherapy is used to treat cancer cells; (i) external radiotherapy that affect surrounding healthy tissues in addition to the tumor area. (ii) the radionuclide therapy which include the use of radioisotopes such as holmium ( $^{166}\text{Ho}$ ), yttrium ( $^{90}\text{Y}$ ) and rhenium ( $^{186}\text{Re}$ ,  $^{188}\text{Re}$ ) which restricts the radiation to a localised tumor area (Hamoudeh, Salim, Barbos, Paunoiu, & Fessi, 2007) (Hafeli U. , Magnetically modulated therapeutic systems, 2004).

## 1.7 Radiation Chemistry

Radiation chemistry is the study of the chemical effects of radiation produced by  $\alpha$ -,  $\gamma$ -,  $\beta$ - rays, electrons, protons, deuterons, neutrons and electro-magnetic radiation of X-rays with energy greater than about 50 eV (Spinks & Woods, 1908)

Radiation Chemistry has a very long history that starts with the discovery of X-rays by Röntgen in 1895. This is followed by the discovery of radioactivity by Becquerel in 1896. Later, in 1898, by comparing the amount of ionization produced by various uranium minerals and salts, Mme. Curie discovered polonium and radium (Hughes, 1973).

The earliest reactions of ionizing radiations were observed by Becquerel in 1896, which was the blackening of a photographic plate exposed to uranium. The decomposition of water containing radium salts by Mme. Curie and A. Debierne in 1901 and the formation of ozone in oxygen irradiated with  $\alpha$ -particles by S. C. Lind in 1912 (Mozumder, 1999).

There are two types of radiation sources namely isotope sources and machine sources. Isotope sources provide continuous radiation and divided into two as naturally occurring or artificially produced.

Some of radioactive isotopes used in radiation chemistry are shown in Table 1 with their half life, radiation and energy.

SOURCE	HALF LIFE	RADIATION	ENERGY (MeV)
<b>Naturally occurring</b>			
Polonium, <sup>210</sup> Po	138 days	$\alpha$	5.304
Radium, <sup>226</sup> Ra	1620 years	$\alpha$	4.777
Radon, <sup>222</sup> Rn	3.83 days	$\alpha$	5.49
<b>Artificially produced</b>			
Cesium, <sup>137</sup> Cs	30 years	$\beta$	0.52
		$\gamma$	0.662
Cobalt, <sup>60</sup> Co	5.27 years	$\beta$	0.314
		$\gamma$	1.332
		$\gamma$	1.173
Tritium, <sup>3</sup> H	11.26 years	B	0.018
Phosphorus, <sup>32</sup> P	14.22 days	B	1.710
Strontium, <sup>90</sup> Sr	28 years	B	0.544
Sulfur, <sup>35</sup> S	87.2 days	B	0.167

**Table 1 Radioactive Isotope Commonly Used as Sources of Radiation**

## 1.8 Imaging Agents

### 1.8.1 Technetium

Technetium is a chemical element with atomic number 43 and symbol Tc. It is a radioactive element and placed in the seventh group of the periodic table.

In 1872, Dmitri Mendeleev predicted many of technetium's properties before the element was discovered. He gave the element the provisional name ekamanganese(Em).

Then, at the same time when Rhenium was discovered, there were some claims about the element 43. Noddack and coworkers thought that they had discovered the element and called it masurium but then nothing more was heard of it (Colton, 1965).

Discovery of Technetium is done by Perrier and Segre in 1937. They showed that radioactivity is obtained when molybdenum is bombarded with deuterons for some month, as being due to the element 43. Later, the element is named as Technetium, from the Greek word artificial as it was the first previously unknown element obtained artificially (Peacock, 1966).

Perrier and Segre also discovered isotopes of Technetium, which are technetium-95 and technetium-97 and have half lives of 60 and 90 days respectively. After discovery of these isotopes, technetium-99 was also synthesized. Most of the chemistry of element 43 is based on technetium-99 (Peacock, 1966).

The Technetium 99m,  $^{99m}\text{Tc}$  nuclear isotope is used for medical imaging as it has half life of 6h and  $\gamma$ -ray emission energy of 141 keV (Dilworth & Parrott, 1998).

Isotope	Preparation	Half-life
$^{93}\text{Tc}$	$^{92}\text{Mo} (p,\gamma) ^{93\text{m}}\text{Tc}$	43.5 min
$^{95\text{m}}\text{Tc}$	$^{95}\text{Mo} (p,n) ^{95\text{m}}\text{Tc}$	61 days
$^{96\text{g}}\text{Tc}$	$^{93}\text{Nb} (\alpha,n) ^{96\text{g}}\text{Tc}$	4.3 days
$^{97}\text{Tc}$	$^{97}\text{Mo} (d,2n) ^{97}\text{Tc}$	$2.6 \times 10^6$ years
$^{97\text{m}}\text{Tc}$	$^{96}\text{Ru} (n,\gamma) ^{97}\text{Ru}, ^{97\text{m}}\text{Tc}$	91 days
$^{98}\text{Tc}$	$^{98}\text{Mo}(p,n) ^{98}\text{Tc}$	$4.2 \times 10^6$ years
$^{99}\text{Tc}$	Fission of U (6.2%)	$2.111 \times 10^5$ years
$^{99\text{m}}\text{Tc}$	$^{98}\text{Mo}(n,\gamma)^{99}\text{Mo}, ^{99\text{m}}\text{Tc}$	6.01 hours

**Table 2 Isotopes of Technetium**

### 1.8.2 Rhenium

Rhenium is a chemical element with atomic number 75 and symbol Re. It is placed in the third row and seventh group of the periodic table.

Existence of this undiscovered element first had been predicted by Dmitry Mendeleev.

W. Noddack and I. Tacke examined ores of neighbouring elements including niobium, molybdenum, tantalum and platinum metals. In 1925, they obtained the X-ray spectrum of element 75 from a gadolinite concentrate and platinum mineral concentrates (Peacock, 1966).

Independently, Loring and Druce confirmed its presence in manganese compounds and Heyrovsky and Dolejsk in commercial manganese salts by polarography (Peacock, 1966).

$^{185}\text{Re}$  (37.4 %) and  $^{187}\text{Re}$  (62.6%) are the two non-radioactive isotopes of Rhenium that occur naturally.

In nuclear medicine, radioactive isotopes,  $^{186}\text{Re}$  and  $^{188}\text{Re}$  are used. Properties of these isotopes are given below (Dilworth & Parrott, 1998).

Isotope	Half life (h)	Max $\beta$ energy (MeV)	$\gamma$ energy keV
$^{186}\text{Re}$	90	1.07 (71%)	137 (9%)
$^{188}\text{Re}$	17	2.12 (100%)	155 (15%)

**Table 3 Radioactive Isotopes of Rhenium**

Rhenium 188 is suitable for therapeutic purposes because of its short-lived beta-emitting property. It has a half life of 16.9h which is suitable for tumor treatment but does not affect the whole body.  $^{188}\text{Re}$  has  $\beta$  radiation with a maximum energy of 2.12 MeV which is effective in tumor therapy and average penetration range of 2.6 mm. It can destroy tumor cells up to a maximum range of 11 mm in tissue beyond which  $\beta$ -electrons are completely attenuated and present no danger to adjacent organs and healthy tissue. In addition Re has  $\gamma$ -energy of 155 keV (15%) which is close to that of Tc and can be easily imaged with a  $\gamma$ -camera (Hafeli, Pauer, Failing, & Tapolsky, 2001) (Wunderlich, et al., 2000).

## **1.9 Aim of this study**

In this study, preparation of magnetite nanoparticles by thermal decomposition method is performed. Small sized, mono dispersed and homogeneous nanoparticles will be synthesized. Two different methods with two different iron precursors will be carried out. In the preparation of magnetite nanoparticles, effect of iron precursor, reaction time, reflux time and ratio of iron precursor: oleic acid will be investigated. In the second part of this study, Rhenium Carbonyl complex will be synthesized. To characterize and prove the formation of nanoparticles and complex, necessary characterization studies will be carried out.

## CHAPTER 2

### EXPERIMENTAL

All the reagents used in experiments were of analytical- reagent grade. De-ionized water obtained from a Millipore water purification system was used in sample and standard preparation. All the glassware and plastic ware were cleaned by soaking them in 10% HNO<sub>3</sub> for at least 24 h and then rinsing three times with distilled water and with deionized water.

#### 2.1 Synthesis of Iron Nanoparticles by Thermal Decomposition Method 1

##### 2.1.1 Chemicals and Reagents

- i. **Ferric acetylacetonate, Tris(acetylacetonato)Iron (III), Fe(acac)<sub>3</sub>**, 97%, has been purchased from Fluka
- ii. **1,2 Hexadecanediol, technical grade 90%**, has been purchased from Sigma-Aldrich.
- iii. **Oleic acid, (9Z)-Octadec-9-enoic acid**, analytical standard, has been purchased from Fluka.
- iv. **Oleylamine, (Z)-9-Octadecen-1-amine**, technical grade, 70%, has been purchased from Fluka.
- v. **Diphenylether**, 99%, has been purchased from Sigma-Aldrich.

- vi. **Hexane (C<sub>6</sub>H<sub>14</sub>)**, has been purchased from Riedel- de Haen.
  
- vii. **Ethanol (C<sub>2</sub>H<sub>5</sub>OH)**, has been purchased from Merck KGaA Darmstadt, Germany.
  
- viii. **N<sub>2</sub> gas**, has been purchased from Linde Gas Company.

### 2.1.2 Procedure

353.17 mg of Fe(acac)<sub>3</sub>, 1.2922 g of 1,2- hexadecanediol, 847.39 mg of oleic acid (b.p= 360°C), 802.47 mg oleylamine and 10 mL of benzyl ether were mixed in a three necked flask. Fe(acac)<sub>3</sub> is used as iron precursor, 1,2 hexadecanediol and oleylamine is used as oxidizing agent, oleic acid is used as surfactant and phenyl ether was used as organic solvent. The mixture reaction was heated under mechanical stirring and a flow of N<sub>2</sub> gas until a temperature of 200°C was reached. This temperature was kept for 30 min and then the solution was heated to reflux (298°C) for 30 min in a N<sub>2</sub> atmosphere. At the end, the solution was cooled down to room temperature. Particles were washed with ethanol and precipitated at 7000 rpm, 10 min with centrifugation. Obtained nanoparticles were dispersed in hexane (Roca, Marco, Morales, & Serna, 2007).

In addition to benzyl ether, phenyl ether ( b.p= 254° C) was also used as high boiling solvent in this method.



**Figure 9 Experimental setup for synthesis of magnetic nanoparticles with Thermal Decomposition Method**

## 2.2 Synthesis of Iron Nanoparticles by Thermal Decomposition Method 2

### 2.2.1 Chemicals and Reagent

- i. **Iron pentacarbonyl, pentacarbonyliron, Fe(CO)<sub>5</sub>**, has been purchased from Sigma- Aldrich.
- ii. **Oleic acid**, analytical standard, has been purchased from Fluka.
- iii. **Dibenzylether**, 99%, has been purchased from Sigma-Aldrich.
- iv. **Octyl ether**, 99%, has been purchased from Sigma Aldrich
- v. **Ethanol (C<sub>2</sub>H<sub>5</sub>OH)**, has been purchased from Merck KGaA Darmstadt, Germany.
- vi. **Hexane (C<sub>6</sub>H<sub>14</sub>)**, has been purchased from Riedel- de Haen.
- vii. **N<sub>2</sub> gas**, has been purchased from Linde Gas Company.

### 2.2.2 Procedure

In this method, Fe(CO)<sub>5</sub> was used as the iron precursor, oleic acid as the surfactant and benzyl ether as the solvent. 0.4 mL of Fe(CO)<sub>5</sub> was added to a mixture containing 20 mL of benzyl ether and 2.58 g of oleic acid at 100°C. The resulting mixture was heated to reflux ( 298° C) and kept at that temperature for 1 h. During this process, initial orange color of the solution gradually turned into black and smoke was seen. The solution was cooled to room T. The remaining solution was washed with ethanol

and precipitated at 7000 rpm, 10 min with centrifugation. Obtained nanoparticles were dispersed in hexane (Woo, Hong, & Ahn, 2005).

In addition to benzyl ether, phenyl ether ( b.p= 254° C) was also used as high boiling solvent in this method.

a



b



c



**Figure 10 a. Initial orange color of the solution. b. Smoke can be seen. c. Final black color of the solution**

## 2.3 Synthesis of $[\text{Re}(\text{CO})_3(\text{OH}_2)_3]^+$ Complex

### 2.3.1 Chemicals and Reagent

- i.  **$\text{BH}_3 \cdot \text{NH}_3$ , amino borane complex**, 99.99%, has been purchased from Sigma Aldrich.
- ii.  **$\text{NaReO}_4$ , Sodium  $^{188}\text{Re}$ - perrhenate**, 99.99%, has been purchased from Sigma Aldrich.
- iii. **Phosphoric acid,  $\text{H}_3\text{PO}_4$** , has been purchased from Sigma Aldrich.
- iv. **Carbon Monoxide gas, CO gas**, pure, has been purchased from OKSAN Tibbi Gazlar Üretim Sanayi ve Ticaret Anonim Şirketi.



a



b



c



**Figure 12 a. Filling of vial with CO for 20 min. b. Experimental setup for complex synthesis c. Radiolabeling by adding Re- perrhenate into the vial and incubated in water bath at 70-80°**

## **2.4 Instruments Used in Characterization Studies**

To obtain information about the shape, size and morphology of magnetite nanoparticles, characterization studies were carried out.

To obtain dispersed nanoparticles, vortex and ultrasonic bath was used. Elma S40 H model ultrasonic bath was used in dispersion of nanoparticles.

### **2.4.1 Centrifuge**

Sigma 2-16 model centrifuge with maximum 13500 rpm rotating speed was used to separate precipitated nanoparticles.

### **2.4.2 Field Emission Scanning Electron Microscopy (FE-SEM)**

Quanta 400 F Field Emission Scanning Electron Microscopy (FE-SEM) from FEI was operated at 30 kV at high vacuum at METU Central Laboratory was used for shape and size characterization of nanoparticles. Synthesized nanoparticles were dispersed in hydrocarbon solvents such as hexane and 25  $\mu\text{L}$  of dispersed nanoparticles were dropped on carbon tape on copper grids. Samples were dried on copper grid at room temperature for 24 hours before performing SEM analysis.

### **2.4.3 Transmission Electron Microscopy (TEM)**

JEOL 2100 F Transmission Emission Microscopy (TEM) was operated at 200 kV, at METU Central Laboratory was used for shape and size characterization of nanoparticles. 200 mesh holey carbon coated grid and 200 mesh lacey carbon coated grid were used for analysis. Samples were dried on grid at room temperature for 24 hours before performing TEM analysis.

#### 2.4.4 Fourier Transform Infrared Spectroscopy (FTIR)

Alpha, Bruker model FTIR was used for characterization of nanoparticles in the range of 300 to 4500  $\text{cm}^{-1}$ . KBr pellets were prepared and liquid samples were dropped on the pellet. Prepared pellets were kept in desiccators until analysis.

#### 2.4.5 Energy Dispersive X-Ray Spectroscopy (EDX)

EDX equipped with FE-SEM was used for elemental analysis of magnetite nanoparticles. The sample used for EDX analysis was same as used for FE-SEM analysis.

#### 2.4.6 X-Ray Diffraction (XRD)

Rigaku Miniflex X-Ray diffractometer with Cu source operating at 35 kW and 15mA was used for chemical analysis of Iron Oxide nanoparticles. Data were collected at  $2\theta$  from  $5^\circ$  and  $75^\circ$ , angles that are present in the X-ray scan. For comparison of experimental results with the theoretical ones and decide on type of iron oxide nanoparticle, ICDD X-ray identification cards were used.

Scherrer Equation is used to correlate the size of nanoparticles. In Scherrer Equation;

$$t = 0.9 \lambda / (B \cos \theta)$$

where

$t$  = thickness, the mean particle size

$\lambda$  = wavelength of the incident x-rays

$B$  = the line broadening at half the maximum intensity in radians

$\theta$  = the Bragg angle, half of the diffraction angle,  $2\theta$

“Bragg diffraction occurs when electromagnetic radiation or subatomic particle waves with wavelength comparable to atomic spacing are incident upon a crystalline sample, scattered in a specular fashion by the atoms in the system, and undergo constructive interference in accordance to Bragg's law” (Myers, 2002). In Bragg's Law;

$$2d \sin\theta = n\lambda$$

where

$n$  = an integer determined by the order given

$\lambda$  = the wavelength

$\theta$  = scattering angle

$d$  = interplanar distance between the lattice planes

Bragg's law can be used to obtain , the lattice constant,  $a$  for the crystal structure using the following equation,

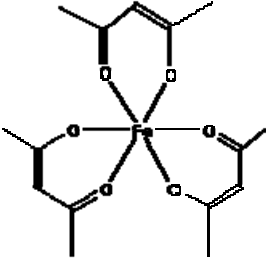
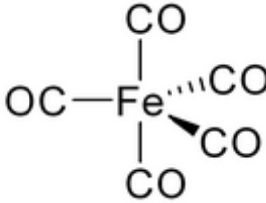
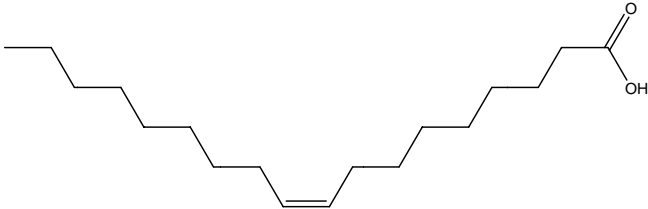
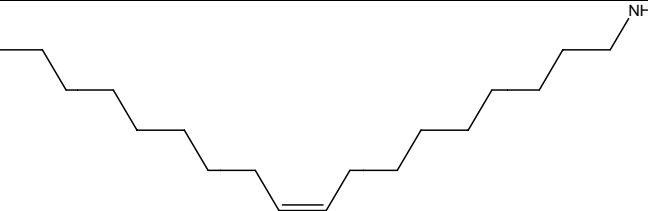
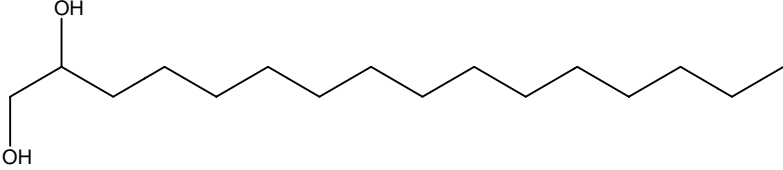
$$d = \frac{a}{\sqrt{h^2 + k^2 + l^2}}$$

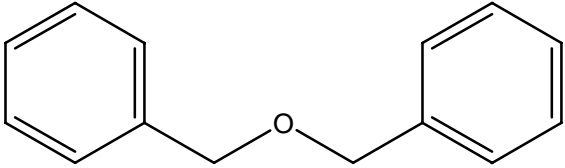
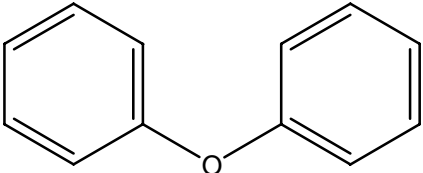
#### **2.4.7 High-Performance Liquid Chromatography- Inductively Coupled Plasma- Mass Spectrometer (HPLC- ICP- MS)**

Dionex, LPG- 3400 A model HPLC equipped Thermo Scientific X series ICP-MS was used for determination of percent conversion of perrhenate to  $[\text{Re}(\text{CO})_3(\text{OH}_2)_3]^+$  Complex. Percent conversion of perrhenate to  $[\text{Re}(\text{CO})_3(\text{OH}_2)_3]^+$  Complex was determined by HPLC- ICP- MS. Both cation exchange column and anion exchange column was tried as a stationary phase. Cation exchange column S5 SCX was used as stationary phase with 10 mM Pyridine Chloride in 5 % MeOH , pH 2.0 as mobile phase with a flow rate of 1.5 mL/min. Anion exchange column S5 SAX was used as stationary phase, 5 mM Sodium Citrate in 10% MeOH , pH 4.5 as mobile phase with

a flow rate of 1.5 mL/ min. It was seen that Anion Exchange Column gave better separation so it was used as a stationary phase during complex determination. Each time approximately 500  $\mu$ L of sample was injected into the system.

## 2.5 Structures of Chemical Compounds Used in Procedures

Name of compound	Structure
Fe(acac) <sub>3</sub>	 <p>The structure shows a central iron atom (Fe) coordinated to three acetylacetonate (acac) ligands. Each acac ligand is a six-membered chelate ring with two oxygen atoms (O) that are coordinated to the iron atom. The ligands are arranged in a propeller-like fashion around the central iron atom.</p>
Fe(CO) <sub>5</sub>	 <p>The structure shows a central iron atom (Fe) coordinated to five carbonyl (CO) groups. The coordination is trigonal bipyramidal: two CO groups are in axial positions (top and bottom), and three CO groups are in equatorial positions (left, right, and back-right). The back-right CO group is shown with a dashed bond, indicating it is behind the plane of the other four.</p>
Oleic acid	 <p>The structure shows a long hydrocarbon chain with a single double bond (cis configuration) and a carboxylic acid group (COOH) at the end. The chain is zig-zagged to represent the carbon atoms.</p>
Oleylamine	 <p>The structure shows a long hydrocarbon chain with a single double bond (cis configuration) and an amine group (NH<sub>2</sub>) at the end. The chain is zig-zagged to represent the carbon atoms.</p>
1,2 hexadecanediol	 <p>The structure shows a long hydrocarbon chain with two hydroxyl groups (OH) attached to the first and second carbon atoms of the chain. The chain is zig-zagged to represent the carbon atoms.</p>

Benzyl ether	
Phenyl ether	

**Table 4 Structures of compounds used in experiments**

## CHAPTER 3

### RESULTS AND DISCUSSION

In this study, mono dispersed, homogeneous and small sized magnetic nanoparticles were synthesized by thermal decomposition method. Synthesized nanoparticles were characterized and then coated with silica for their potential use in tumor imaging. In the second part of the thesis, synthesis of Rhenium carbonyl complex was performed for radiolabeling studies.

#### 3.1 Synthesis of Iron Oxide Nanoparticles by Thermal Decomposition Method

Thermal Decomposition method is used for synthesis of mono dispersed and small particle sized magnetite ( $\text{Fe}_3\text{O}_4$ ) nanoparticles.  $\text{Fe}(\text{acac})_3$  and  $\text{Fe}(\text{CO})_5$  were used as iron precursor in synthesis of these particles. Procedures mentioned in 2.1.2 and 2.2.2 were used for synthesizing nanoparticles by  $\text{Fe}(\text{acac})_3$  and  $\text{Fe}(\text{CO})_5$  respectively.

There are three main factors that influence particle size of magnetite synthesized by thermal decomposition method. These are reaction temperature (boiling point of the solvent used), time and Fe/oleic acid molar ratio.

It is known from literature that for biomedical applications, magnetite would preferred over maghemite because of its higher saturation magnetization and susceptibility. Therefore, although both maghemite and magnetite could be prepared successfully using thermal decomposition method, we focused on the synthesis and characterization of magnetite as these particles were aimed to be used in biomedical applications. Hence,  $\text{N}_2$  gas was purged through reaction medium during the synthesis to prevent oxidation of magnetite to maghemite.

In thermal decomposition methodology, to achieve the required high temperature conditions, high boiling point organic solvents are required. Two different high boiling solvents, phenyl ether and benzyl ether were used in this study. Boiling points of phenyl ether and benzyl ether are 254° C and 298° C respectively. During synthesis, solvent was heated until boiling and kept at that temperature as described in experimental part.

The synthesized nanoparticles can be dispersed in hydrocarbon solvents such as hexane, octane and toluene.

Particle size, shape and morphology of particles were characterized by TEM, FTIR and XRD.

There are some practical considerations in the thermal decomposition method:

When using  $\text{Fe}(\text{CO})_5$  as the iron precursor, it is important to add  $\text{Fe}(\text{CO})_5$  to reaction medium at 100° C as it decomposes at 120° C.

The length of the distillation column used for refluxing was critical. When a distillation column with a length of 14-15 cm was used, most of the solvent was evaporated and reaction was terminated in a short time. Nanoparticles synthesized under this condition, utilizing  $\text{Fe}(\text{acac})_3$  as iron precursor and phenyl ether as the solvent are presented in Figure 13, the reflux time was less than 30 minutes.

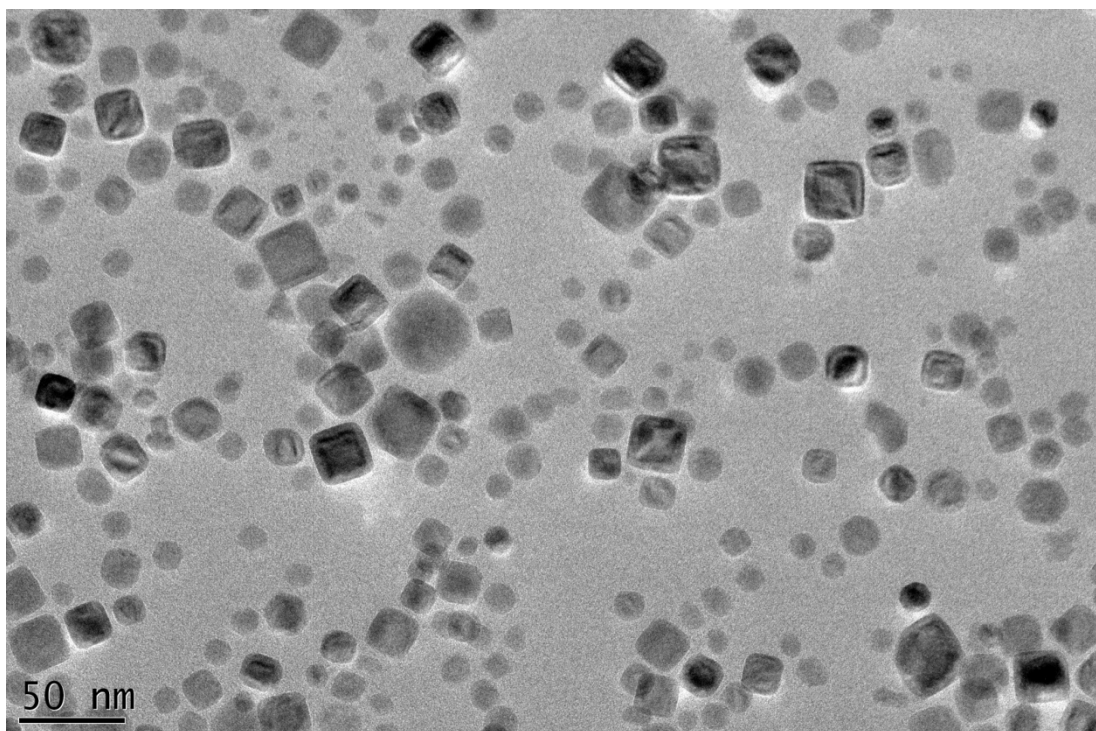


**Figure 13 TEM image of magnetite nanoparticles synthesized by thermal decomposition method. Iron precursor =  $\text{Fe}(\text{acac})_3$ , solvent = phenyl ether, reflux time < 30 minutes,  $\text{Fe}(\text{acac})_3$  : oleic acid = 1:3**

As can be seen from figure, both spherical and cubic nanoparticles were formed. After the usage of a distillation column with a length of 24-25 cm, better size and shape control were obtained.

Washing and precipitation processes were also very important steps due to the usage of large amount of oleic acid. Removing of oleic acid from the reaction medium was a hard process. Several washing cycles were needed. The effect of residual oleic acid in TEM measurements are shown in Figure 14 (Roca, Marco, Morales, & Serna, 2007).

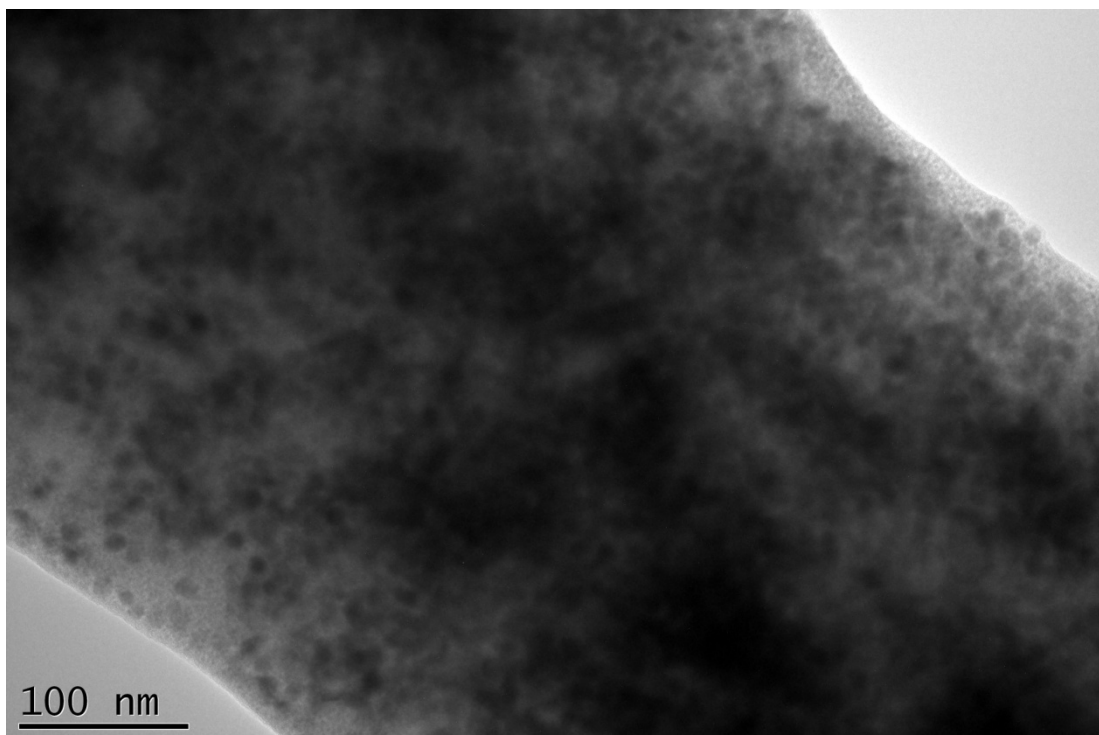


**Figure 14 TEM image of magnetite nanoparticles synthesized by thermal decomposition method. Iron precursor =  $\text{Fe}(\text{acac})_3$ , solvent = phenyl ether, reflux time = 30 minutes,  $\text{Fe}(\text{acac})_3$  : oleic acid = 1:3**

As can be seen from Figure 14, there is a cloud over the particles which prevents visualization of the nanoparticles.

### **3.1.1 Effect of Iron Precursor on Nanoparticle Formation**

Two different iron precursor were used in the production of  $\text{Fe}_3\text{O}_4$  nanoparticles, namely  $\text{Fe}(\text{acac})_3$  and  $\text{Fe}(\text{CO})_5$  and their effects on particle formation were investigated.

TEM images of the two iron oxide samples synthesized by decomposition of these two organic precursors are shown in Figure 15 and Figure 16.

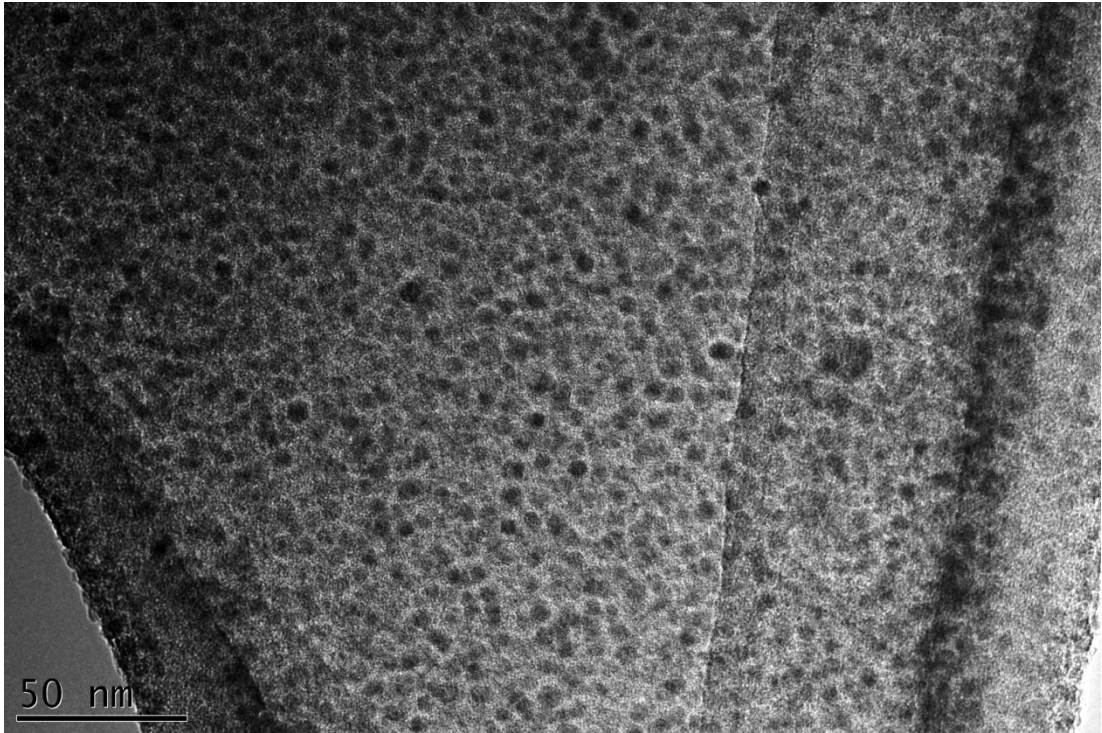


**Figure 15 TEM image of magnetite nanoparticles synthesized by thermal decomposition method. Iron precursor=  $\text{Fe}(\text{acac})_3$ , solvent= phenyl ether, reflux time= 30 minutes,  $\text{Fe}(\text{acac})_3$  : oleic acid= 1:3, N=25, average particle size= 5.55 nm, standard deviation= 0.71**

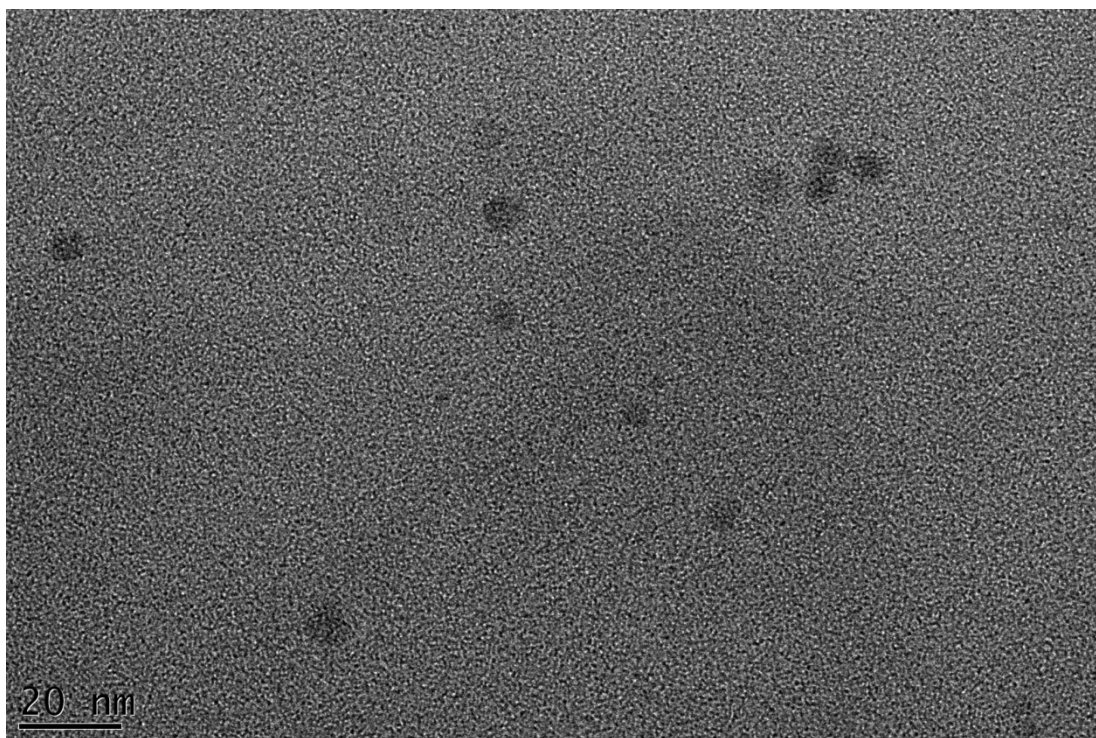


**Figure 16 TEM image of magnetite nanoparticles synthesized by thermal decomposition method. Iron precursor=  $\text{Fe}(\text{CO})_5$ , solvent= benzyl ether, reflux time= 60 minutes,  $\text{Fe}(\text{CO})_5$  : oleic acid= 1:3, N= 15, average particle size= 8.86 nm, standard deviation= 2.91**

These figures show that the samples consist of nanoparticles uniform in size. Formed nanoparticles were isolated one from another due to steric repulsions of the surface bonded oleic acid chains. Nanoparticles produced using iron acetylacetonate as the precursor and phenyl ether as the solvent have a mean average size of 5.55 nm and quasi-spherical shapes.

When iron pentacarbonyl was used as the precursor and benzyl ether as the solvent, the mean particle size was 8.86 nm and the shape was sphere. However, although repeated 3 times, the nanoparticle formation yield of the latter method was very low. This observation might be correlated with the higher decomposition temperature of the iron pentacarbonyl. Probably the heating and refluxing system used in or laboratory was not effective enough for the decomposition of the precursor i.e. a delay in the nucleation of the iron oxide nanoparticles. Which might cause the formation of

only small number of nuclei in the medium at later stages of the reaction. Those few nuclei will grow further forming the observed nanoparticles.

Since the size, morphology and monodispersity of the nanoparticles produced by these two methods were suitable to our goals, the first one (utilizing the acetyl acetate as precursor) that produce large amount of particles was preferred.

### **3.1.2 The Effect of Reaction Temperature (solvent boiling point) on Nanoparticle Formation**

In the previous section, the low yield of the formed particles with iron pentacarbonyl precursor was correlated with the inefficiency of the heating process. Hence, in this section a higher boiling point solvent, benzyl ether ( 298 ° C) was used in both of the synthesis procedures. TEM images of the particles prepared using iron pentacarbonyl and iron acetylacetonate in benzyl ether are shown in Figure 17 and Figure 19, 21 respectively. For comparison, TEM images of the particles prepared using iron pentacarbonyl and iron acetyl acetate in phenyl ether (254°C) are depicted in Figure 23 and Figure 25, 27.

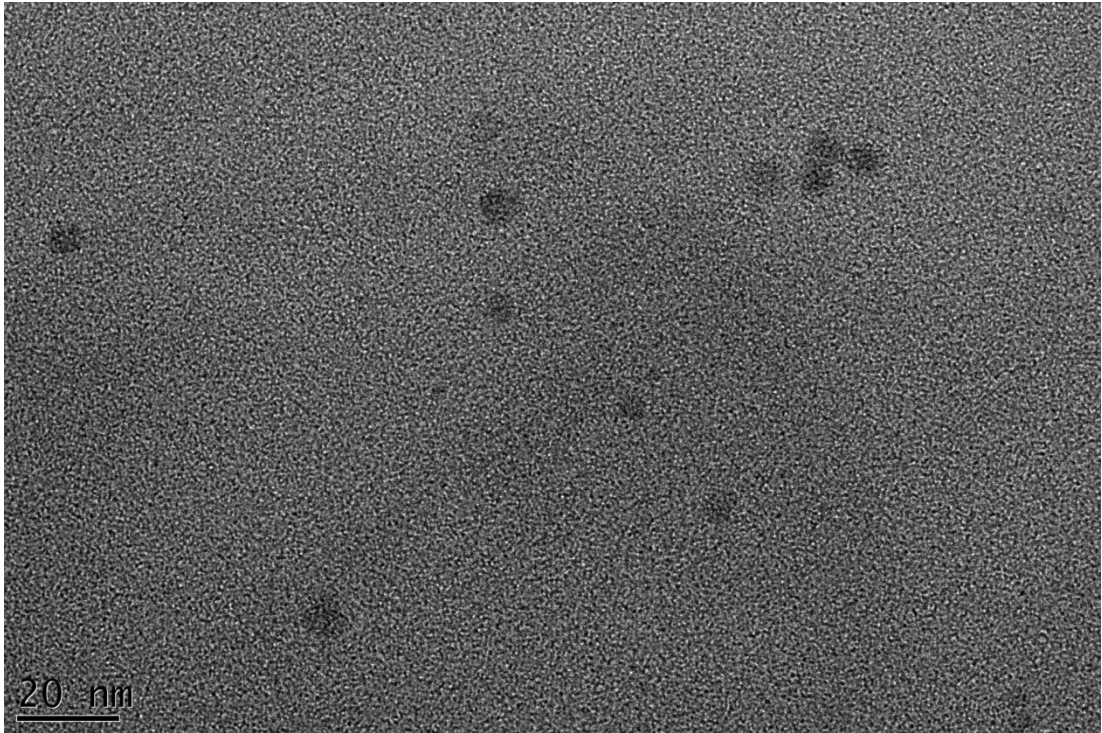


**Figure 17 TEM image of magnetite nanoparticles synthesized by thermal decomposition method. Iron precursor=  $\text{Fe}(\text{CO})_5$ , solvent= benzyl ether, reflux time= 60 minutes,  $\text{Fe}(\text{CO})_5$  : oleic acid= 1:3, N= 12, average particle size= 8.86 nm, standard deviation= 2.91**

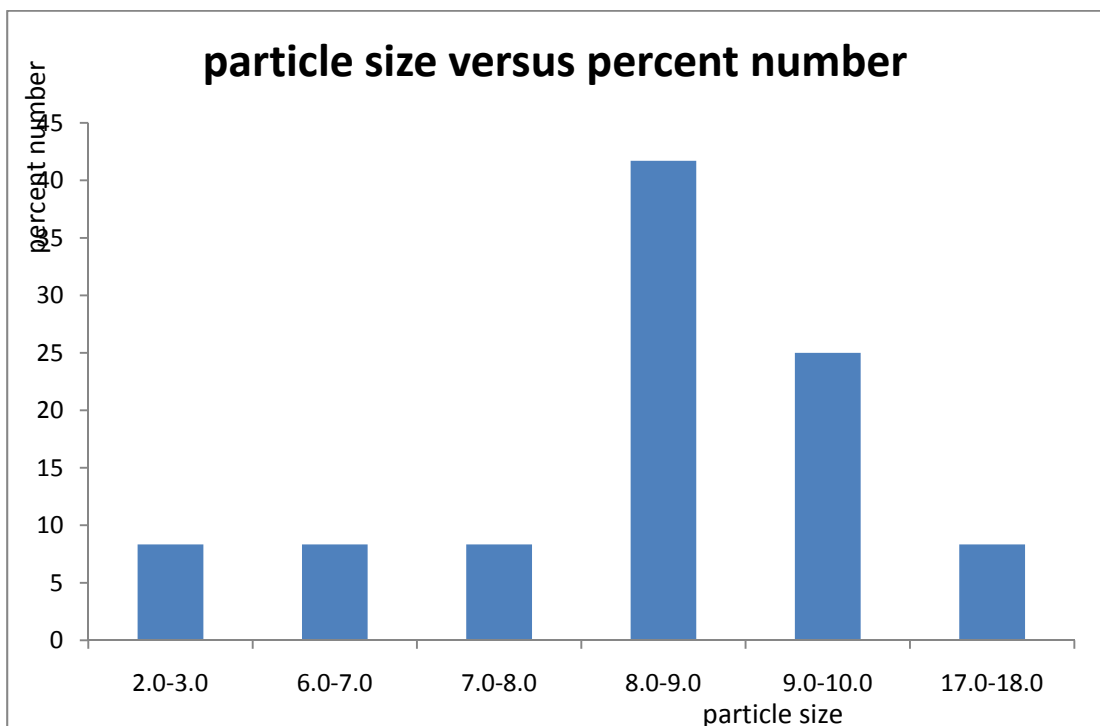


**Figure 18 Particle size versus number of particles diagram of nanoparticles in Figure 17**

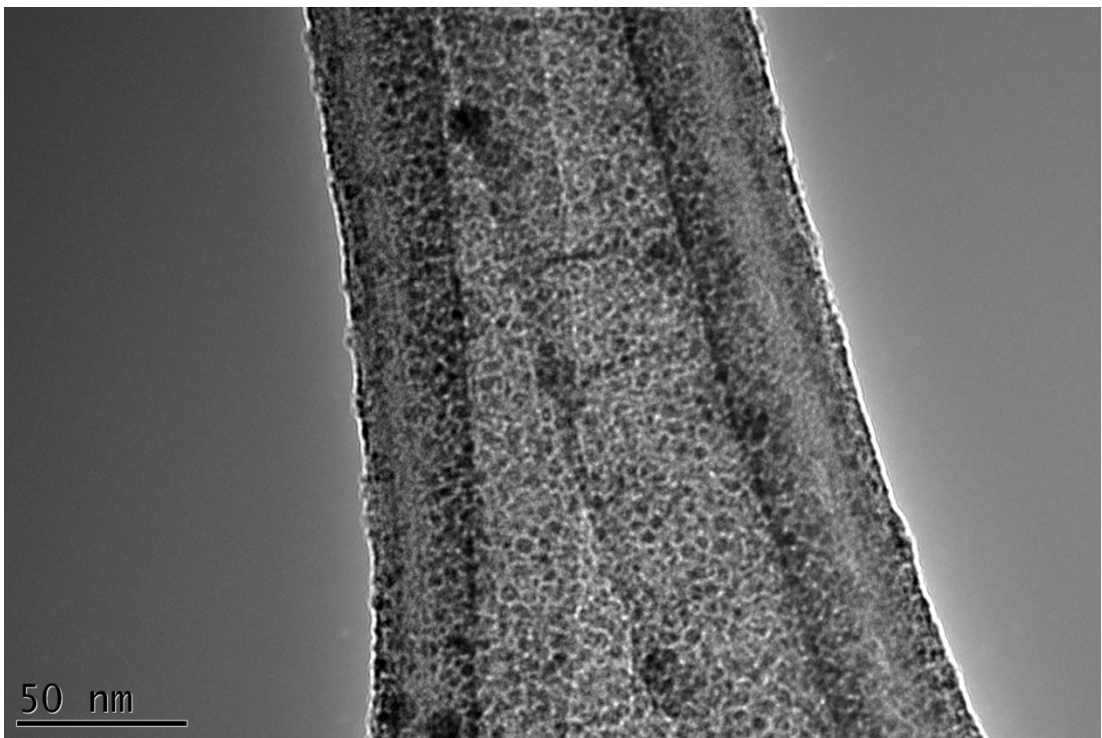


**Figure 19 TEM image of magnetite nanoparticles synthesized by thermal decomposition method. Iron precursor=  $\text{Fe}(\text{acac})_3$ , solvent = benzyl ether, reflux time= 30 minutes,  $\text{Fe}(\text{acac})_3$  : oleic acid= 1:3, N= 25, average particle size= 5.62 nm, standard deviation= 0.54**

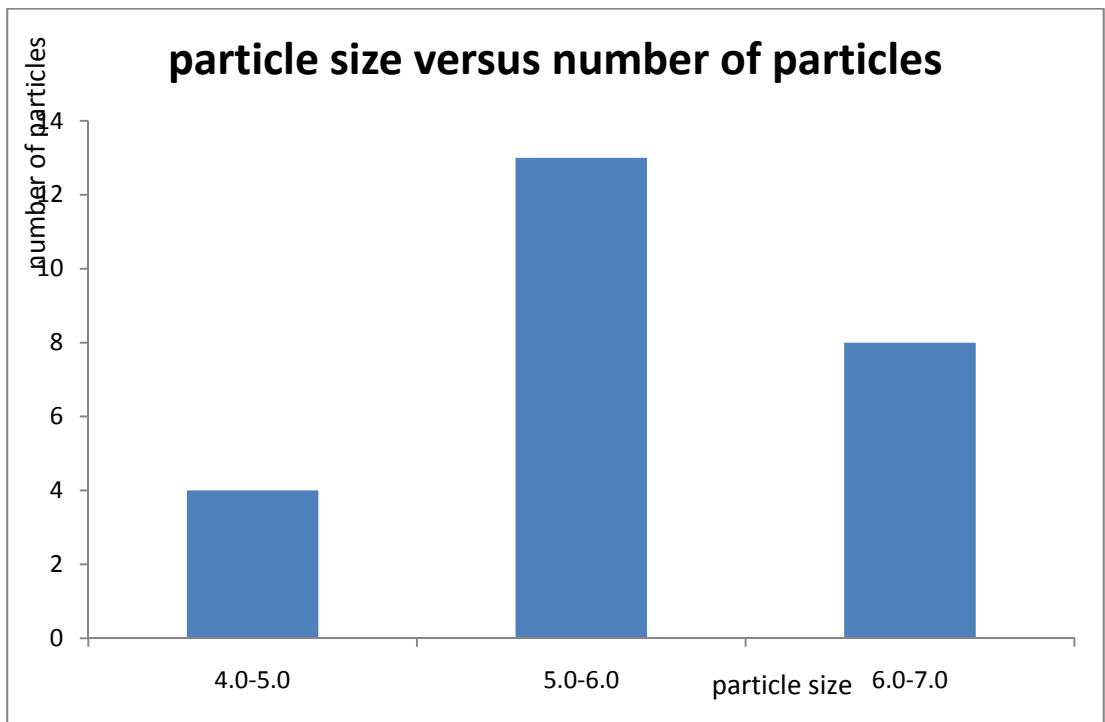


**Figure 20 Particle size versus number of particles diagram of particles in Figure 19**

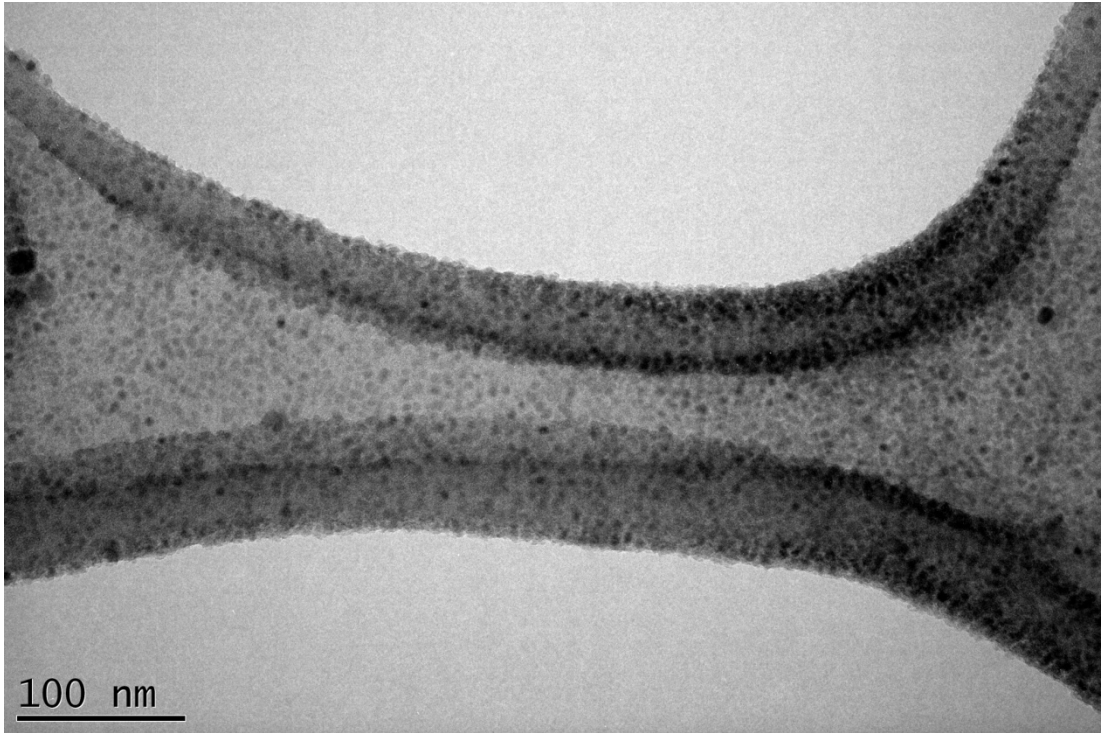


**Figure 21** TEM image of magnetite nanoparticles synthesized by thermal decomposition method. Iron precursor=  $\text{Fe}(\text{acac})_3$ , solvent= benzyl ether, reflux time= 30 minutes,  $\text{Fe}(\text{acac})_3$  : oleic acid= 1:3, N=25, average particle size= 6.53 nm, standard deviation= 1.03

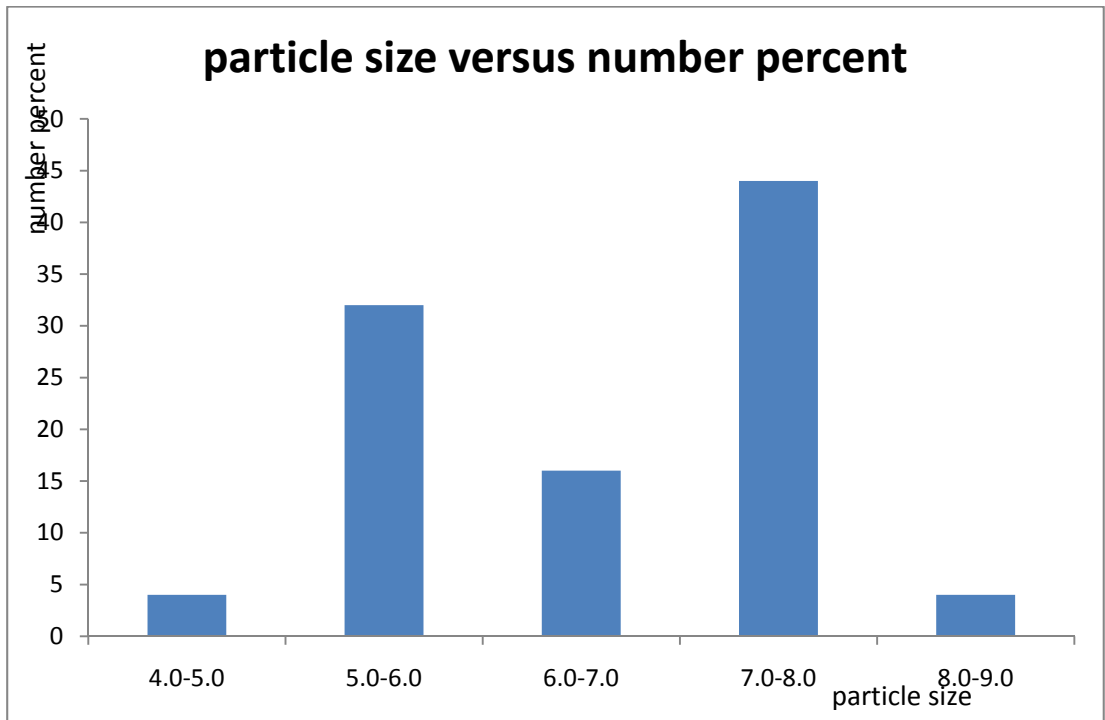


**Figure 22** Particle size versus number of particles diagram of particles in Figure 21

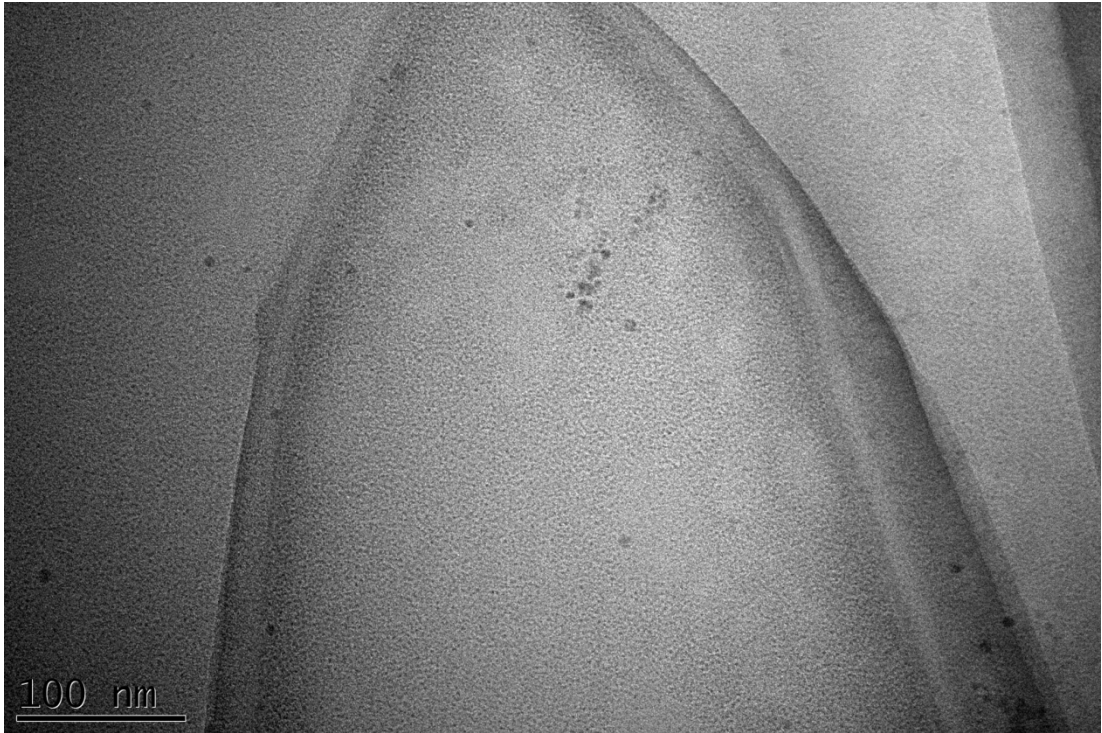


**Figure 23** TEM image of magnetite nanoparticles synthesized by thermal decomposition method. Iron precursor=  $\text{Fe}(\text{CO})_5$ , solvent = phenyl ether, reflux time= 60 minutes,  $\text{Fe}(\text{CO})_5$  : oleic acid= 1:3, N=25, average particle size= 7.40 nm, standard deviation= 2.21

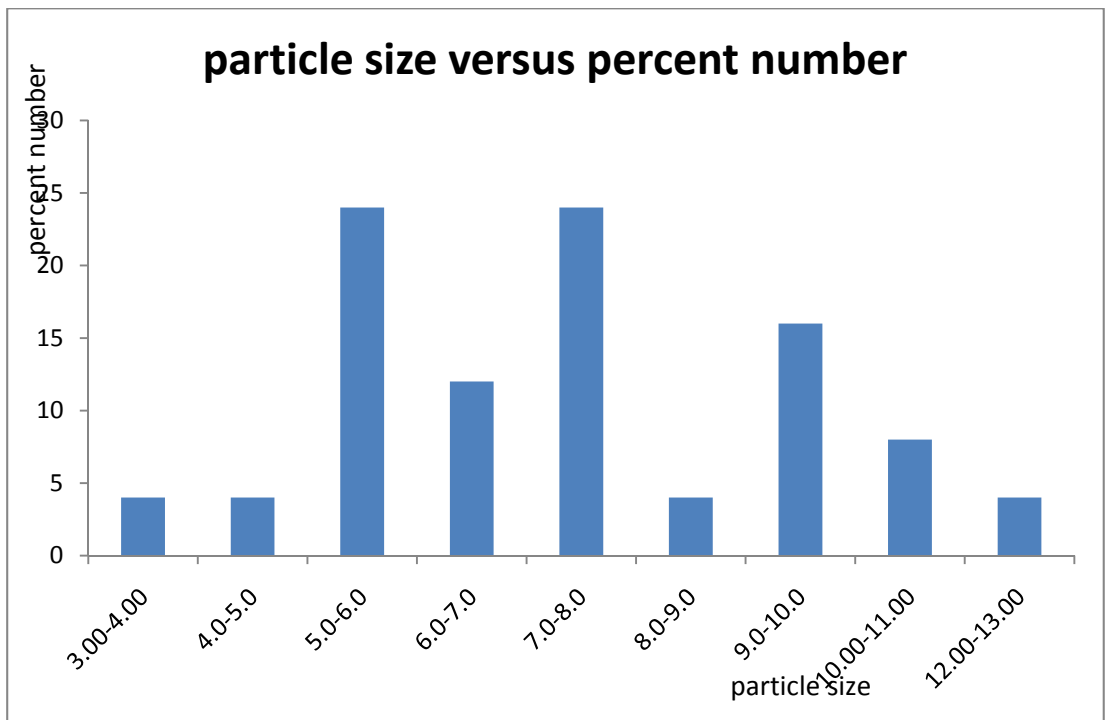


**Figure 24** Particle size versus number of particles graph of particles in Figure 23

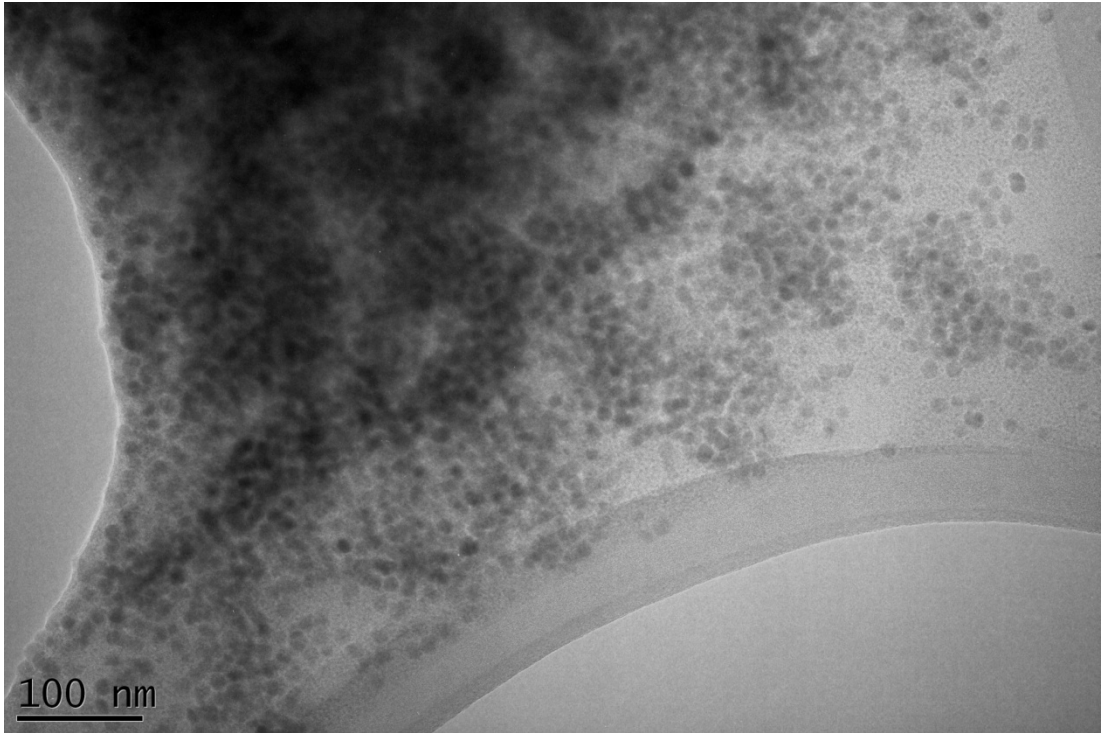


**Figure 25** TEM image of magnetite nanoparticles synthesized by thermal decomposition method. Iron precursor=  $\text{Fe}(\text{acac})_3$ , solvent = phenyl ether, reflux time = 30 minutes,  $\text{Fe}(\text{acac})_3$  : oleic acid = 1:3,  $N=25$ , average particle size = 7.65 nm, standard deviation= 1.23

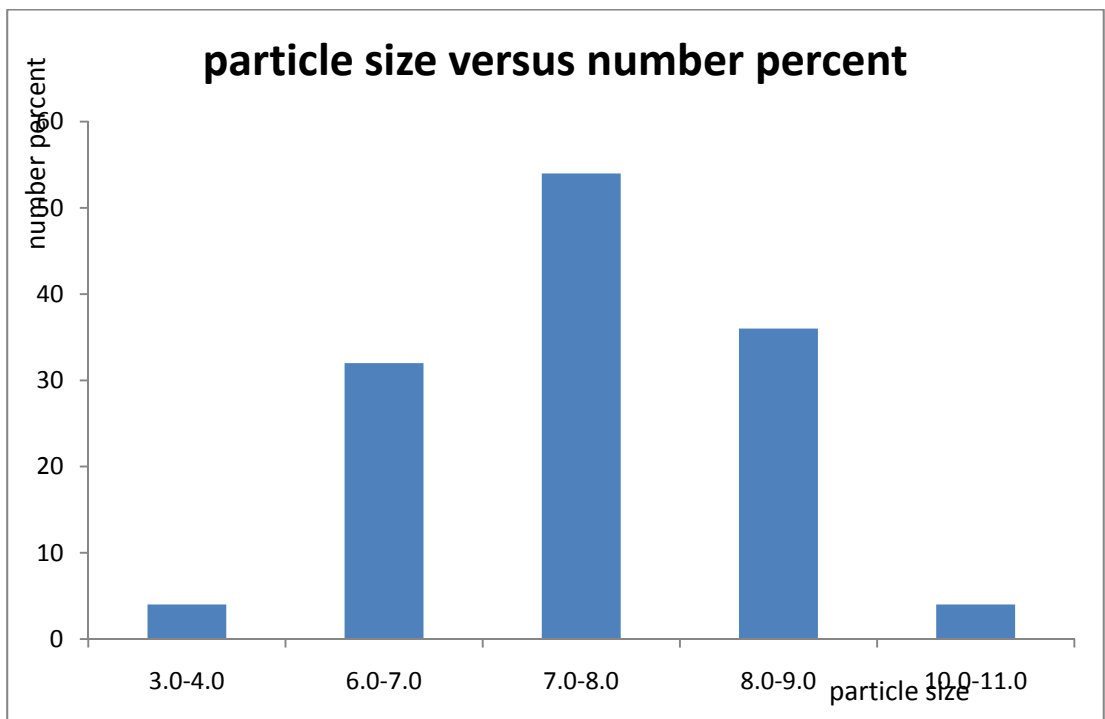


**Figure 26** Particle size versus number percent graph of Figure 25

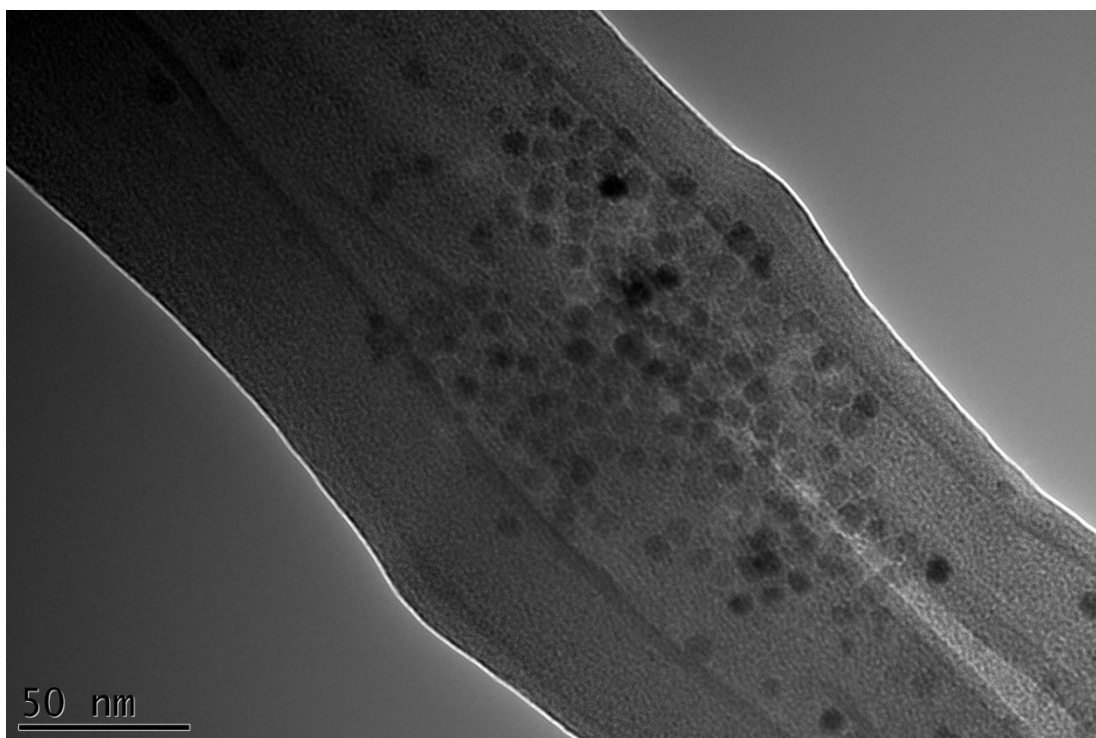


**Figure 27 TEM image of magnetite nanoparticles synthesized by thermal decomposition method. Iron precursor=  $\text{Fe}(\text{acac})_3$ , solvent = phenyl ether, reflux time = 30 minutes,  $\text{Fe}(\text{acac})_3$  : oleic acid = 1:3,  $N=25$ , average particle size = 7.97 nm, standard deviation= 1.44**

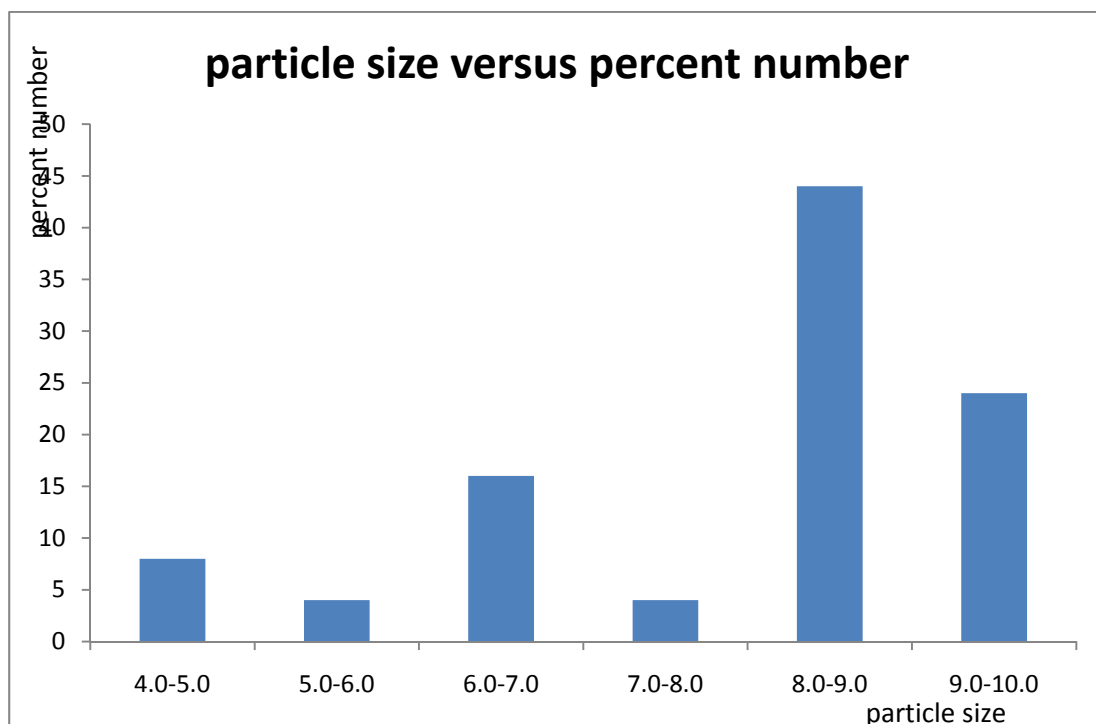


**Figure 28 Particle size versus percent number of particles in Figure 27**

As can be seen from the figures, particles (<10 nm) prepared by both of two solvents have very uniform size distribution. However, as noticed from the TEM images also, the yield of the particles prepared in the presence of benzyl ether was higher than that of phenyl ether. In pentacarbonyl case although the number of particles produced was increased, the yield was still much smaller compared to iron acetyl acetonate method. Therefore, the use of iron acetyl acetonate precursor in benzyl ether medium was decided to be used in the preparation of the nanoparticles by thermal decomposition method.

### 3.1.3 The Effect of Reflux Time on Particle Formation

Both the nucleation and the growth steps of the particle formation requires some time. On the other hand, the growth process should be quenched at appropriate times; otherwise thermodynamically more stable shapes may form. Hence the duration of the reaction was varied in between 15-60 minutes. A quasi-cube-shape nanocrystals were observed as the common products, Figure 29, when the reaction was terminated after 15 minutes. Nikhil and coworkers have also observed the formation of quasi-cube-shape nanocrystals at the early stage of their reaction when they were following the iron oxide nanocrystal formation steps through thermal decomposition. They have claimed that the cubes were much more stable and readily observable when a high concentration of a fatty acid with a relatively long chain was used as the ligands as in our case (Jana, Chen, & Peng, 2004).

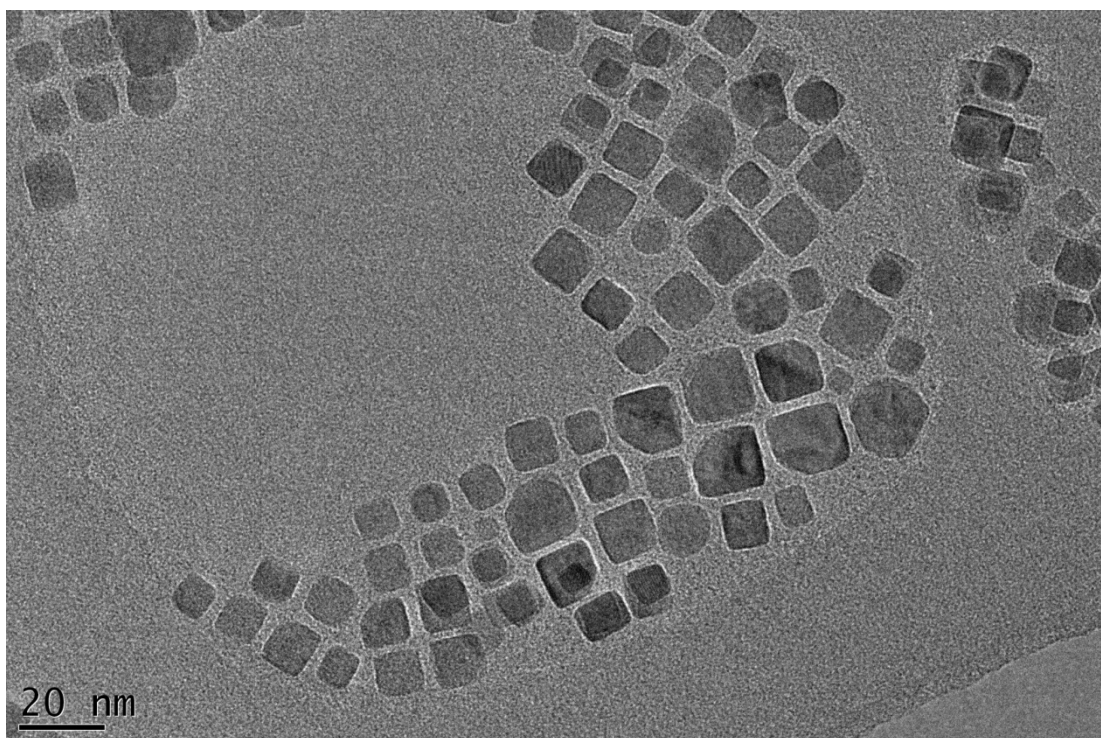


**Figure 29** TEM image of magnetite nanoparticles synthesized thermal decomposition method. Iron precursor=  $\text{Fe}(\text{acac})_3$ , solvent = phenyl ether, reflux time < 30 minutes,  $\text{Fe}(\text{acac})_3$  : oleic acid = 1:3

As the reaction time was extended to 30 minutes, the shape of the nanoparticles was turned into sphere (Figure 29).

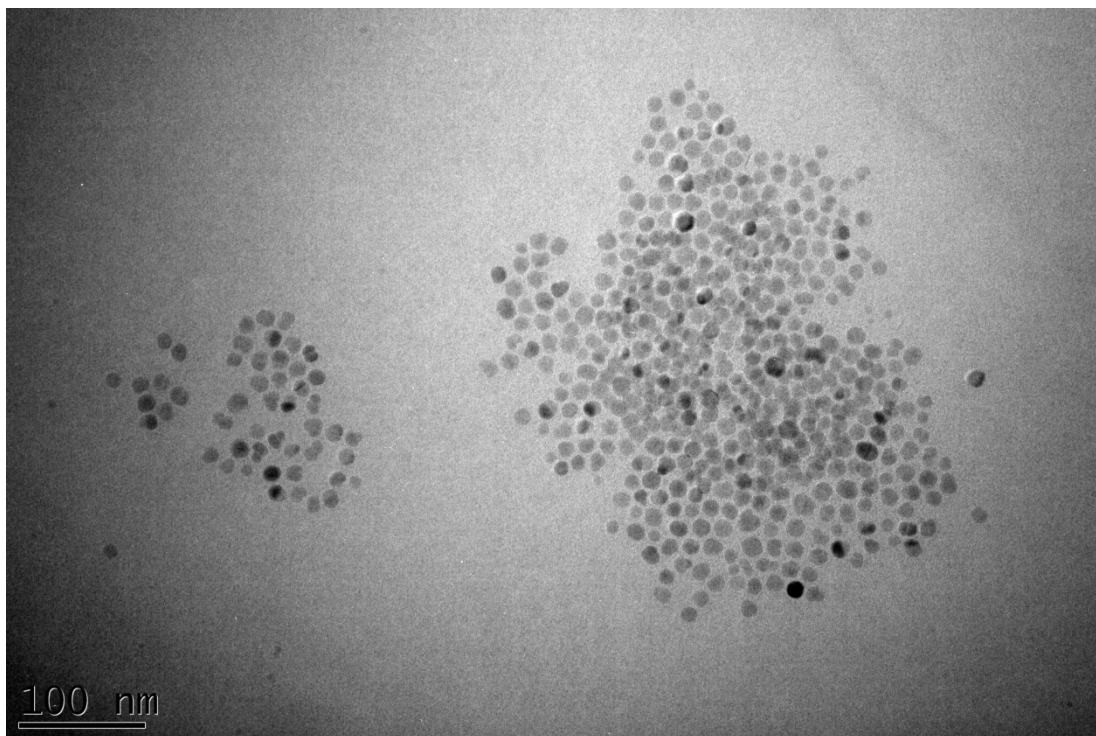


**Figure 30. TEM image of magnetite nanoparticles synthesized by thermal decomposition method. Iron precursor=  $\text{Fe}(\text{acac})_3$ , solvent = phenyl ether, reflux time = 0 minutes,  $\text{Fe}(\text{acac})_3$  : oleic acid = 1:3**

As can be seen in Figure 30, mono dispersed, small size, sphere shape nanoparticles were obtained. It has been stated by Nikhil and coworkers that this conversion occurs probably through intraparticle ripening because, in their study the volumes of cubes and the spheres were almost the same (Jana, Chen, & Peng, 2004).

When the reflux time was changed into 60 minutes, larger particles were started to appear around small ones (Figure 31) probably due to Ostwald ripening process.

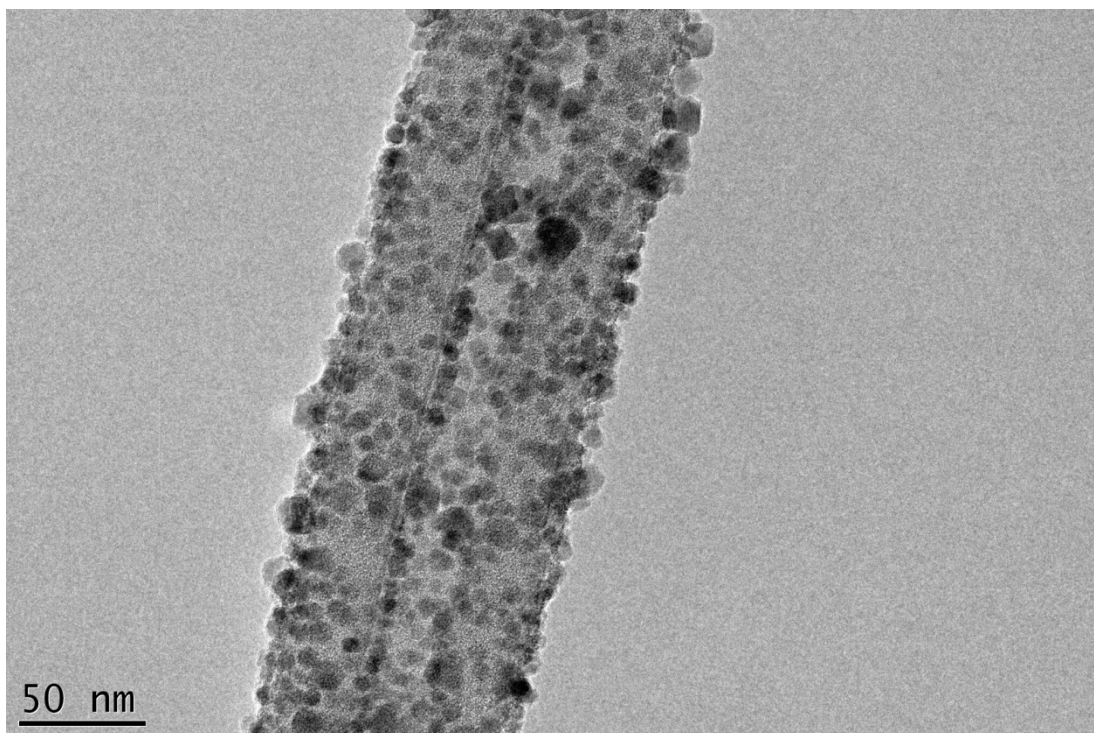


**Figure 31** TEM image of magnetite nanoparticles synthesized by thermal decomposition method. Iron precursor =  $\text{Fe}(\text{acac})_3$ , solvent = benzyl ether, reflux time = 60 minutes,  $\text{Fe}(\text{acac})_3$  : oleic acid = 1:3

In our studies, the time window for the nanoparticle formation, determined by the chain length and/or concentration of the ligands, was confined in a time range which was longer than 15 and shorter than 60 minutes. Regarding the mono dispersity and morphology of the nanoparticles obtained at the reaction time of 30 minutes, it was selected as the optimum value without performing any other experiments. One point should be emphasized here. The reflux system should not be left unattended during particle preparation. Otherwise possible change of the reaction volume, would directly affect the particle monodispersity and morphology.

### 3.1.4 Effect of Iron Precursor to Oleic Acid Ratio

According to Hyeon et al. when ratio of iron precursor,  $\text{Fe}(\text{CO})_5$  to oleic acid is changed, size of the nanoparticles change. They have obtained 4, 7 and 11 nm particles by varying the ratio as 1:1, 1:2, and 1:4 respectively. (Hyeon, Lee, Park, Chung, & Hyon, 2001).

In our study, the effect of the ratio of  $\text{Fe}(\text{acac})_3$  to oleic acid was investigated. When the starting reaction mixture containing 1:1, 1:3 and 1:5 molar ratios were used in the synthesis,  $\text{Fe}_3\text{O}_4$  nanoparticles with particle sizes of 4.05, 5.55 and 6.52. were obtained, respectively. Average particle sizes were calculated by selecting 50 particles randomly, measuring their diameter and taking their average value. TEM images of the particles obtained with a ratio of 1:1, 1:3 and 1:5 are given in Figures 32, 34 and 36.

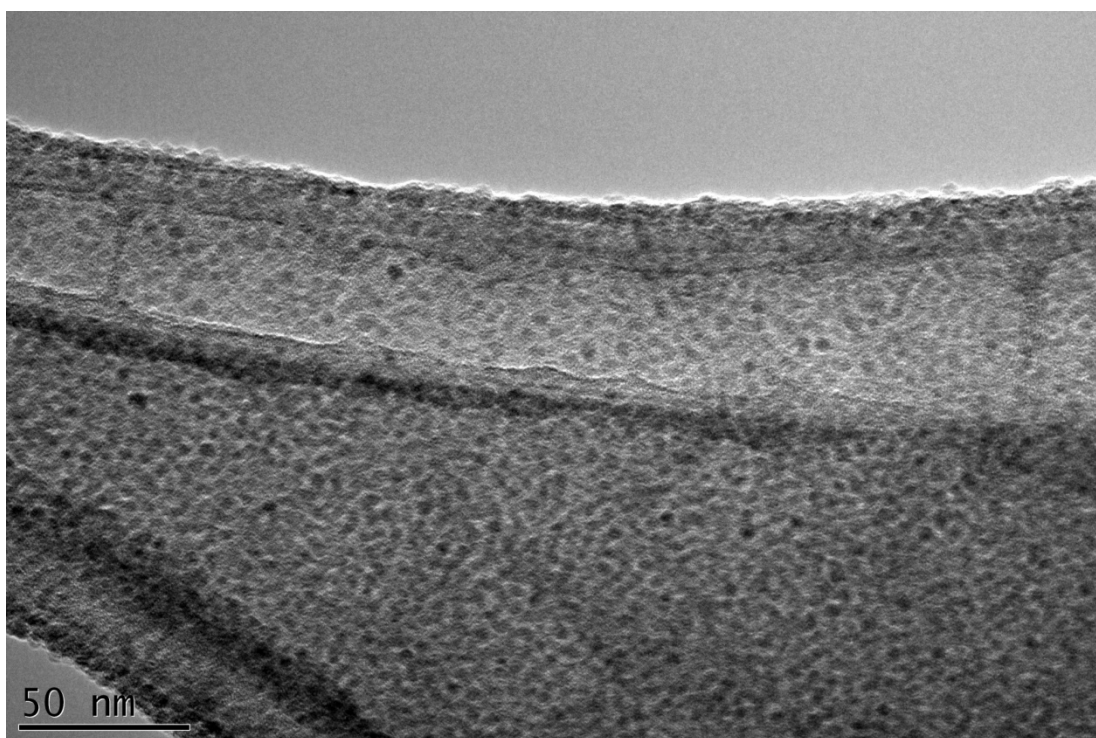


**Figure 32. TEM image of magnetite nanoparticles synthesized by thermal decomposition method. Iron precursor =  $\text{Fe}(\text{acac})_3$ , solvent = benzyl ether, reflux time = 30 minutes,  $\text{Fe}(\text{acac})_3$  : oleic acid = 1:1, N=25, average particle size = 4.03 nm, standard deviation= 0.69**

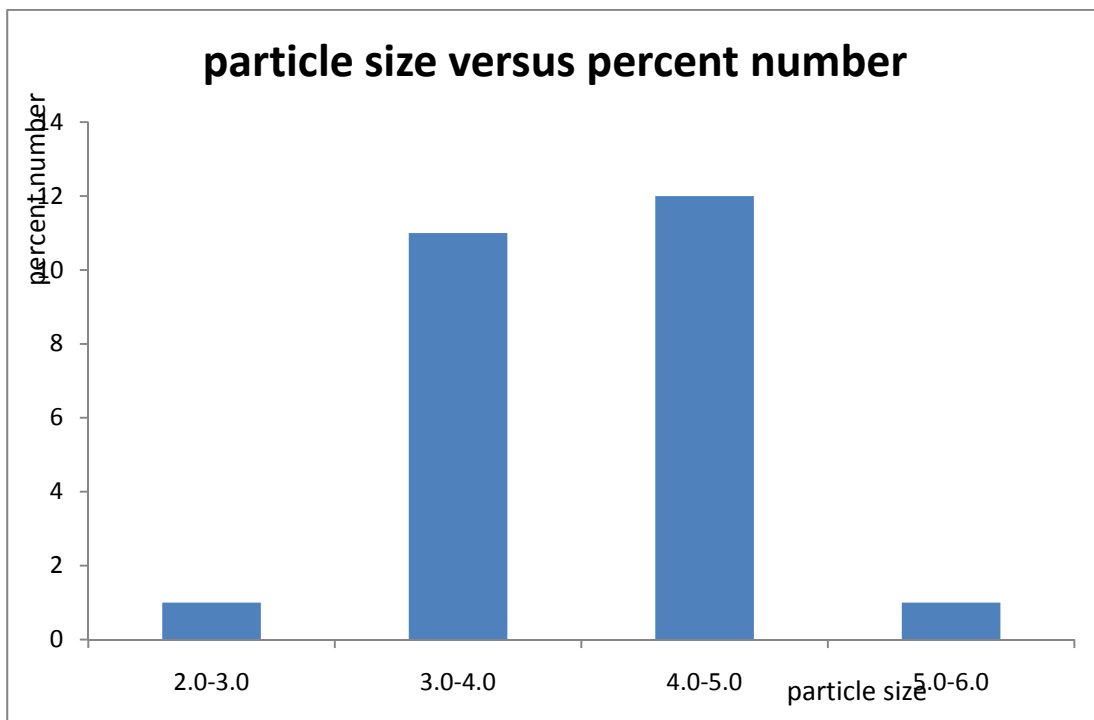


**Figure 33 Particle size versus percent number graph of Figure 30**

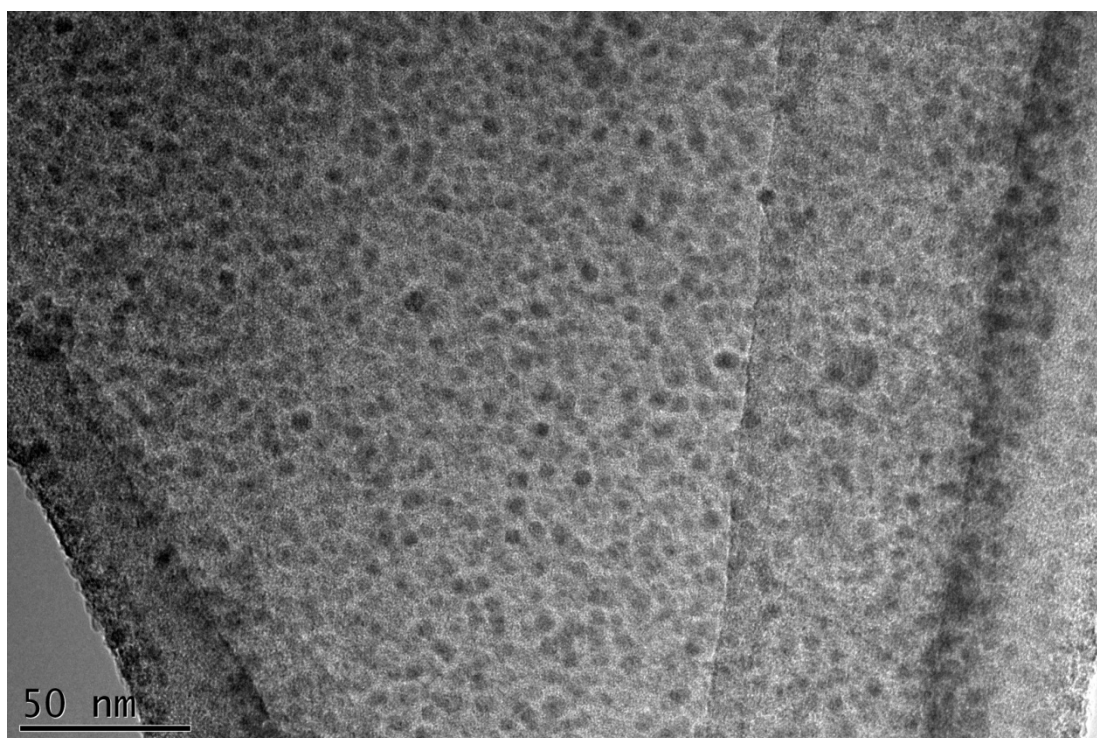


**Figure 34. TEM image of magnetite nanoparticles synthesized by thermal decomposition method. Iron precursor =  $\text{Fe}(\text{acac})_3$ , solvent = benzyl ether, reflux time = 30 minutes,  $\text{Fe}(\text{acac})_3$  : oleic acid = 1:3, N=25, average particle size = 5.55 nm, standard deviation= 0.71**

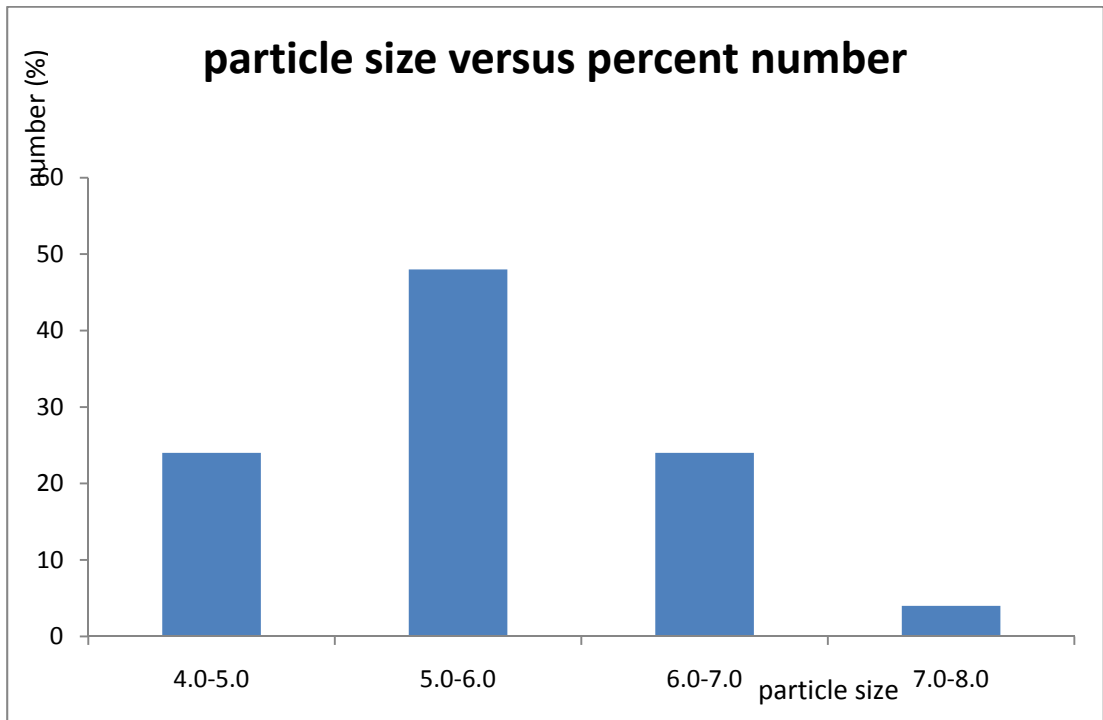


**Figure 35 Particle size versus percent number diagram of Figure 31**

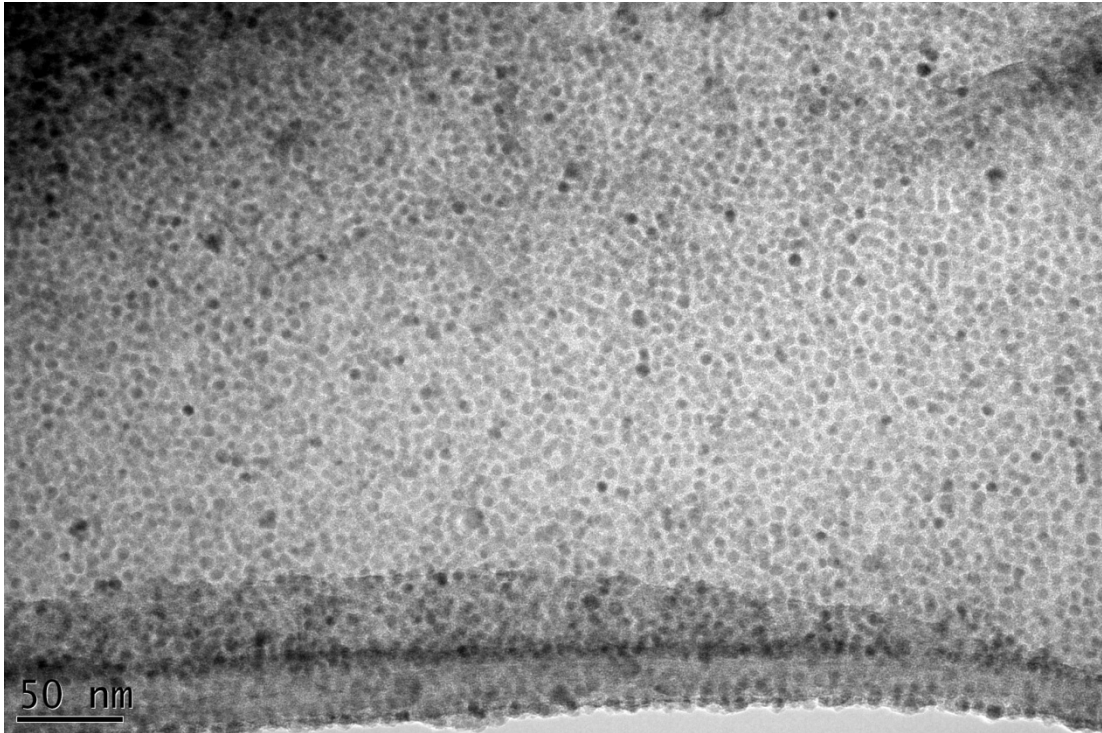


**Figure 36. TEM image of magnetite nanoparticles synthesized by thermal decomposition method. Iron precursor =  $\text{Fe}(\text{acac})_3$ , solvent = benzyl ether, reflux time = 30 minutes,  $\text{Fe}(\text{acac})_3$  : oleic acid = 1:5,  $N=50$ , average particle size = 6.52 nm, standard deviation= 0.92**

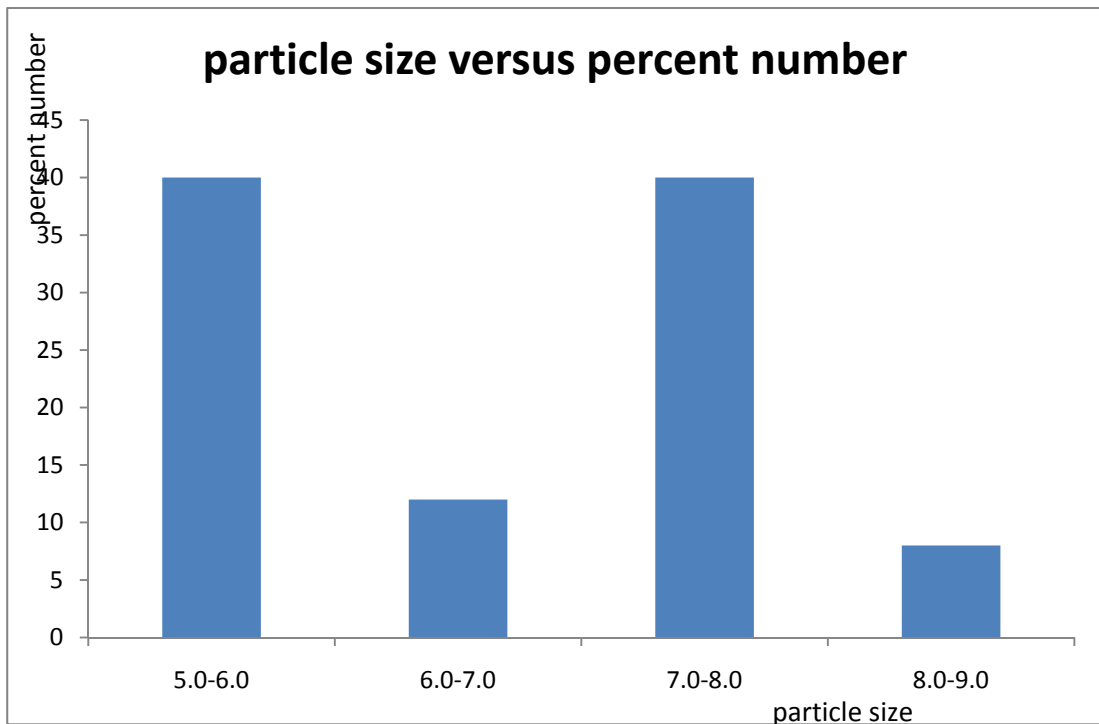


**Figure 37 Particle size versus number of particles diagram of Figure 33**

As can be seen from figures, the particles are all, mono disperse, spherical in shape and self assembled.

Particle size analysis of nanoparticles was also performed. As can be seen from below graph, particle size versus percent volume graph was correlated with the results that we obtained from TEM images.

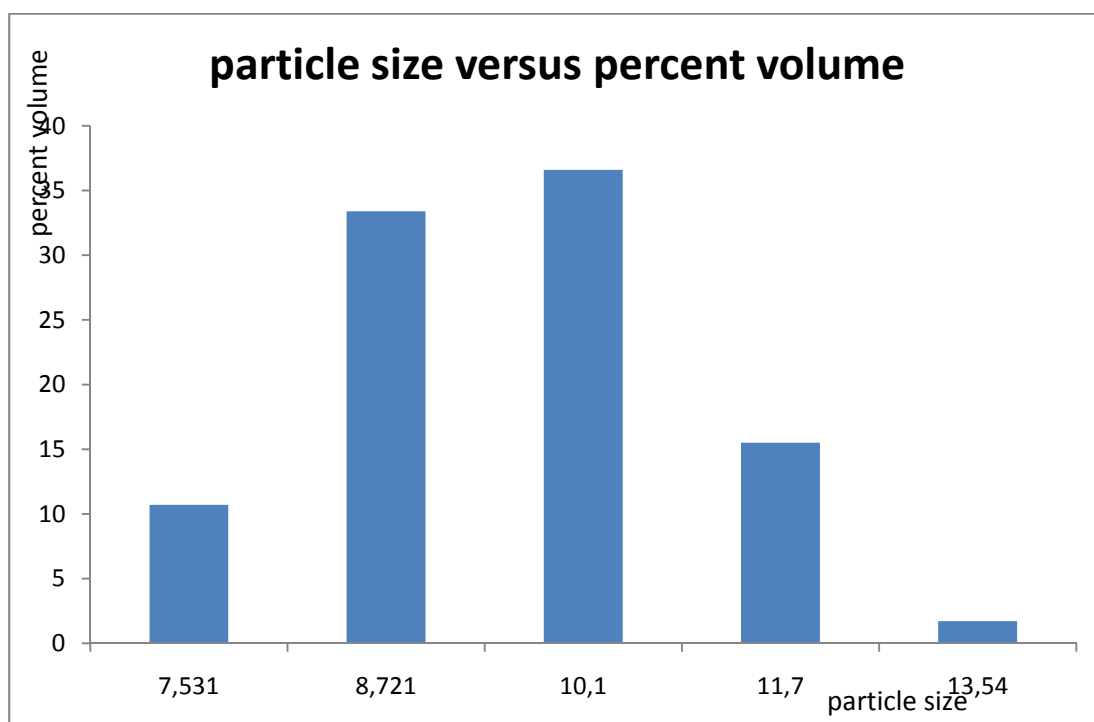


**Figure 38 Particle size distribution curve of magnetite nanoparticles that is synthesized by  $\text{Fe}(\text{acac})_3$  and benzyl ether.**

### 3.1.5 IR Studies

Particles were also characterized by FT-IR. FT-IR spectrum of particles shows the chemical bonds of  $\text{Fe}_3\text{O}_4$ . FT-IR spectrum of nanoparticles is shown in Figure 39.

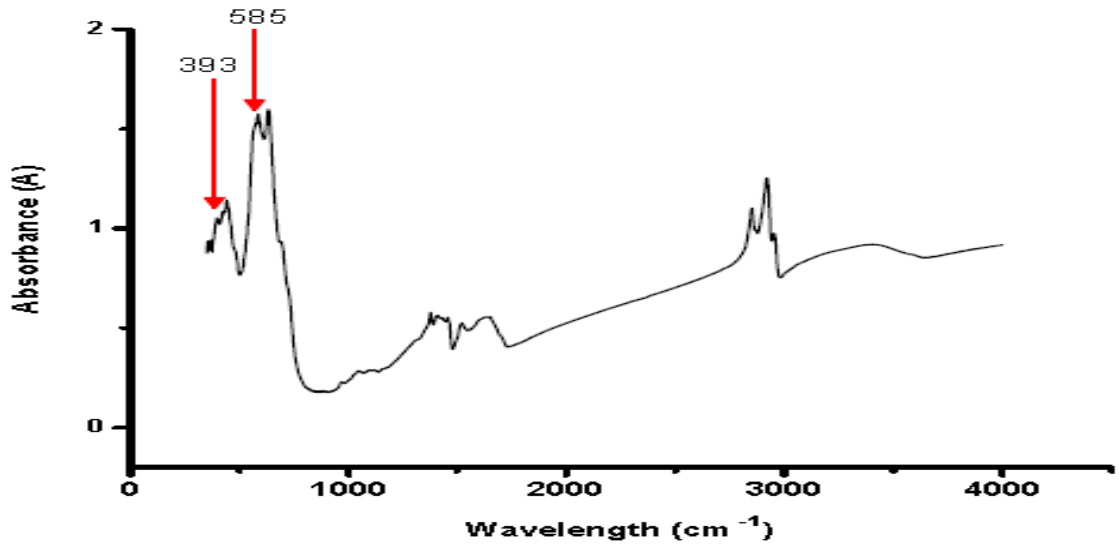


**Figure 39 FT-IR spectrum of  $\text{Fe}_3\text{O}_4$  nanoparticles.**

In Figure 39, the peaks at 393 and 585  $\text{cm}^{-1}$  were assigned to Fe-O stretching modes of the magnetite lattice. The results were in accordance with the values mentioned by Serna and coworkers (Roca, Marco, Morales, & Serna, 2007) .

### 3.1.6 Magnetic Properties of Synthesized Magnetite Nanoparticles



5 min after synthesis



30 min after synthesis



1 h after synthesis



2 h after synthesis

**Figure 40 Pictures of magnetite nanoparticles after 5 minute, 30 minute, 1hour and 2 hours after the synthesis**

Figure 40 shows the pictures of nanoparticles in hexane after 5 minutes, 30 minutes, 1 hour and 2 hours after the synthesis. As can be seen from pictures although powerful external magnet is present, there is no change in solution even after 2 hour. This may be an indication of superparamagnetism. In addition to that black color of the solution is the indication of magnetite instead of maghemite.

### 3.1.7 XRD Measurements of the Iron Oxide Nanoparticles

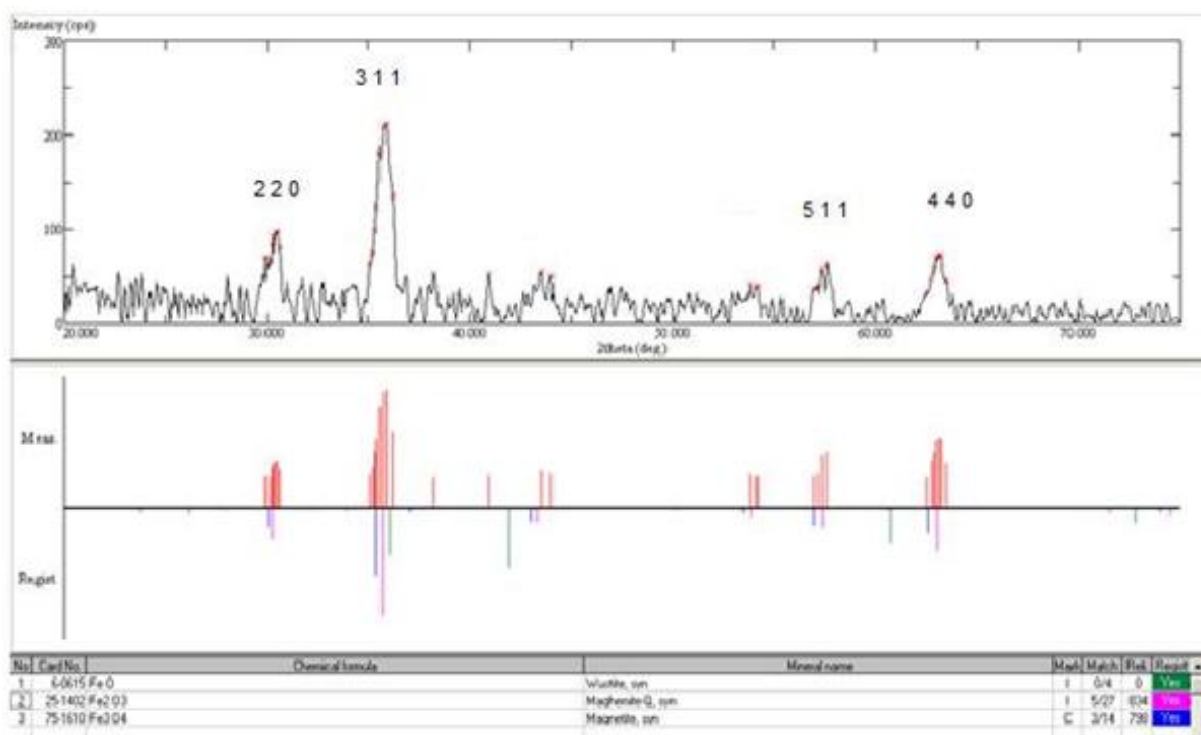


**Figure 41 X- Ray Diffraction pattern of two week magnetite nanoparticles prepared by phenyl ether and Fe(acac)<sub>3</sub>**

The XRD pattern of the nanoparticles prepared by Fe(acac)<sub>3</sub> and phenyl ether was illustrated in Figure 41. All detected diffraction peaks could be attributed to the

characteristic peaks of spinel oxide ( $\square$ -  $\text{Fe}_2\text{O}_3$  or  $\text{Fe}_3\text{O}_4$ ) according to ICDD X-ray identification cards.

The lattice constant,  $a$ , of the sample was calculated as 0.840 nm from the most intense peaks according to Bragg's Law. The lattice constants of maghemite ( $\square$ -  $\text{Fe}_2\text{O}_3$ ) and magnetite ( $\text{Fe}_3\text{O}_4$ ) are reported as 0.835 nm and 0.839 nm, respectively. The main crystalline phase of synthesized sample could be identified as a mixture of magnetite and maghemite when the calculated and theoretical lattice constants,  $a$  and the interplanar distances,  $d$  matched. The result can be seen in Table 5.

**Table 5 Theoretical (ICDD Card No: 75-1610) and measured crystal parameters of two weeks magnetite nanoparticles.**

(h k l)	Measured $2\theta$ ( $^\circ$ )	Theoretical $d_{hkl}$	Calculated $d_{hkl}$	Calculated $a(\text{nm})$
(2 2 0)	30.35	2.095	2.94251	0.832
(3 1 1)	35.4	2.5309	2.53346	0.840
(4 4 0)	62.95	1.484	1.47523	0.835
(5 1 1)	62.75	1.615	1.47945	0.834

By using XRD spectrum and Scherrer's equation that is mentioned in 2.4.6, average size of two week stored nanoparticles can be estimated. In size determination of nanoparticles, most intense peak of the pattern, 3 1 1 is used. According to the XRD pattern in Figure 41, average size of nanoparticles is calculated as 8.5 nm.

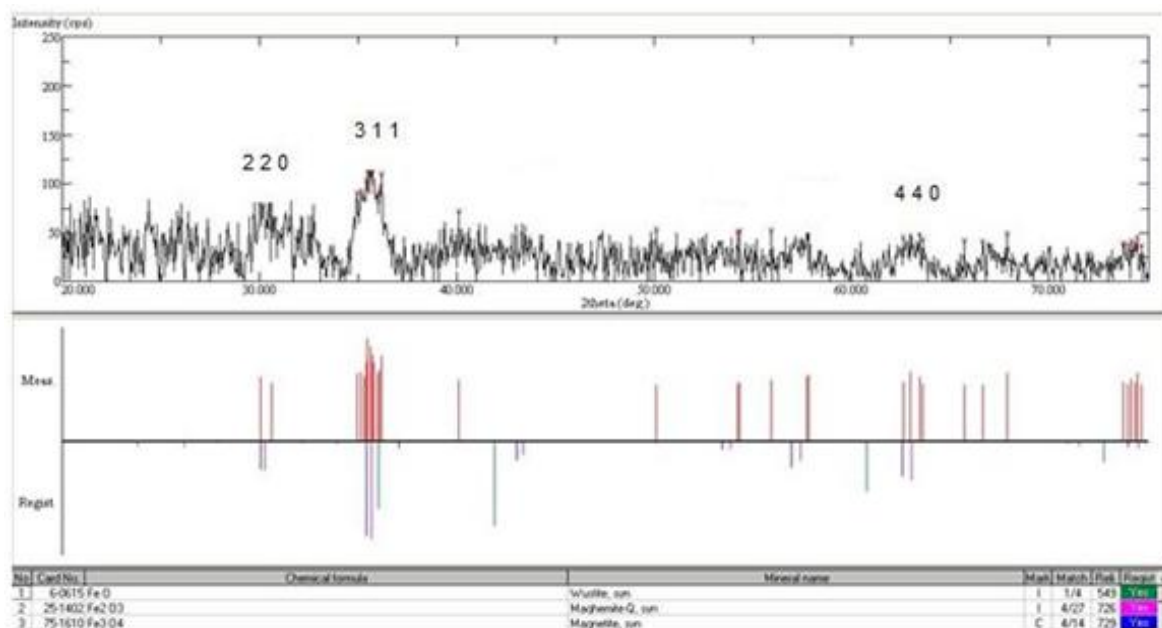


**Figure 42 X- Ray Diffraction pattern of two weeks magnetite prepared by benzyl ether and Fe(acac)<sub>3</sub>**

The XRD pattern of the nanoparticles prepared by Fe(acac)<sub>3</sub> and benzyl ether was illustrated in Figure 42. All detected diffraction peaks could be attributed to the characteristic peaks of spinel oxide (□- Fe<sub>2</sub>O<sub>3</sub> or Fe<sub>3</sub>O<sub>4</sub>) according to ICDD X-ray identification cards.

The lattice constant, a , of the sample was calculated again as 0.840 nm from the most intense peaks according to Bragg's Law. The main crystalline phase of synthesized sample could be identified as a mixture of magnetite and maghemite when the

calculated and theoretical lattice constants,  $a$  and the interplanar distances,  $d$  matched. The result can be seen in Table 6.

**Table 6 Theoretical (ICDD Card No: 75-1610) and measured crystal parameters of two weeks magnetite nanoparticles.**

(h k l)	Measured $2\theta$ (°)	Theoretical $d_{hkl}$	Calculated $d_{hkl}$	Calculated $a$ (nm)
(2 2 0)	30.05	2.099	2.9712	0.840
(3 1 1)	35.3	2.5309	2.54041	0.840
(4 4 0)	62.95	1.484	1.47523	0.835

Again by using Scherrer's equation, average size of nanoparticles can be estimated. In size determination of nanoparticles, most intense peak of the pattern 3 1 1 is used. According to the XRD pattern in Figure 42, average size of nanoparticles is calculated as 5.7 nm.

### 3.2 Synthesis of Re Carbonyl Complex

This thesis is a part of Industry Thesis Projects. This project consists of two thesis. One is done by Ümit Zengin with a name of “Preparation and Characterization of Silica Coated Magnetite Nanoparticles and Labeling with Nonradioactive Re As A Surrogate of Tc-99m for Magnetically Targeted Imaging”. The combination of these two thesis covers the project. In this thesis, synthesis of small and monodispersed nanoparticles was achieved. Synthesis of rhenium carbonyl complex is a part of this study. In the synthesis of Re carbonyl complex, Ümit Zengin and I worked together.

Reductive carboxylation is a process in which metallic radionuclide is attached to a molecule that is used in targeting to obtain a kinetically stable nuclide. The tricarbonyl  $MCO_3^+$  (M= Re or Tc) is a metallic nuclide and can be synthesized according to below reaction, Figure 43.

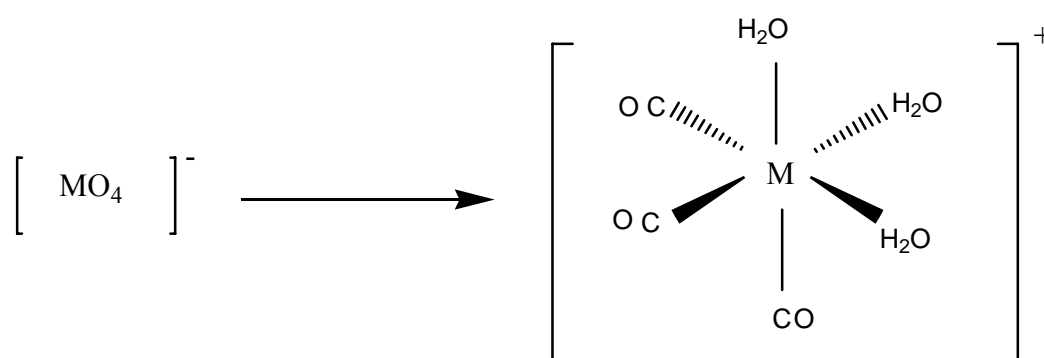


**Figure 43. Metal Tricarbonyl formation by reductive carboxylation**

$NaBH_4$  is a reducing agent that is frequently used in metal center carboxylation reaction. A major disadvantage of  $NaBH_4$  is that hydrolyzation of it takes place very fast in acidic medium. For this reason, in carboxylation of Re,  $NaBH_4$  is replaced by  $BH_3NH_3$  which is water-soluble, highly reducing and stable under neutral/ acidic conditions (Schibli, et al., 2002).

For the synthesis of Rhenium Carbonyl complex, some important points should be emphasized. First, particle size of  $\text{BH}_3\text{NH}_3$  should be very small and well spread during flushing of  $\text{CO}(\text{g})$  to give it property of holding more  $\text{CO}(\text{g})$ . For this,  $\text{BH}_3\text{NH}_3$  should be grounded well in a mortar and sieved with a sieve. As  $\text{BH}_3\text{NH}_3$  holds more  $\text{CO}(\text{g})$ , it directly increase the yield of complex formation as it increases the number of  $\text{CO}$  reacted with reduced rhenium.

As it was mentioned above, reduction of rhenium is took place in an acidic medium. The acidity of the medium is another parameter in rhenium carbonyl synthesis. It is observed that at least 60  $\mu\text{L}$  of  $\text{H}_3\text{PO}_4$  was needed for reduction of rhenium.

During the synthesis, the reaction of water with aminoborane brings out hydrogen gas.  $\text{H}_2$  gas should be balanced with a syringe to keep the system pressure balanced.

In literature, mostly radioactive rhenium was used for reductive carboxylation of rhenium. The efficiency of complex formation is detected by thin layer chromatography (TLC) or HPLC equipped with gamma ray counter.

In this study, nonradioactive isotope of Rhenium was used. For determination of rhenium carbonyl complex, firstly perrhenate solution and synthesized rhenium carbonyl complex solution were runned on a TLC plate and results are tried to be visualized by a UV lamp. Eriochrome Black T was used as indicator in visualization of spots under UV lamp. When an organic solvent is present, TLC plate fluoresces in the presence of an organic compound as it contains a fluorophore. However, no result were taken from TLC so HPLC-ICP-MS was used to visualize the formation and measurement of the amount of complex formation. In this instrument, firstly rhenium carbonyl complex was separated from the perrhenate by HPLC and their amount in the effluent were measured by ICP-MS.

### 3.2.1 Optimization Studies

To optimize the conditions and increase the yield of complex formation, some parameters were changed and change in yield of complex formation was followed using HPLC- ICP- MS.

Parameters changed during optimization studies were acidity, type of vial used, CO(g) flushing time and particle size of the  $\text{BH}_3\text{NH}_3$  used.

Acidity of the medium is one of the parameters that affect complex formation. As the acidity of the medium was increased two times, from 30  $\mu\text{L}$  to 60  $\mu\text{L}$ , yield of complex formation increases 28%.

Type of vial used was another parameter that affects complex formation. As the interaction of CO(g) with  $\text{BH}_3\text{NH}_3$  is important, impermeability and volume of the vial is very important. The vial used should be small and capped properly to have a suitable interaction of  $\text{BH}_3\text{NH}_3$  used.

$\text{BH}_3\text{NH}_3$  is another parameter that affects complex formation. It should be grounded well in order to obtain small sized  $\text{BH}_3\text{NH}_3$ . As the size of  $\text{BH}_3\text{NH}_3$  decreases, interaction of it with CO increases.

To follow the change of yield of complex formation, HPLC- ICP- MS was used. Both cation exchange column and anion exchange column were used in this study.

When cation exchange column was used, S5 SCX cation exchange column was used as a stationary phase. 10 mM pyridine chloride solution in 5.0% EtOH at pH 2.0 was used as the mobile phase with a flow rate of 1.5 mL/min.

As can be seen in Figure 44, rhenium complex is retained in the cation exchange column and its signal is seen later than the negatively charged  $\text{ReO}_4^-$  on the chromatogram. As can be seen from the figure,  $\text{ReO}_4^-$  with green gives only one signal, blank solution with red gives no signal, complex solution except CO(g) with purple gives same signal as  $\text{ReO}_4^-$  as no formation of complex is present and lastly complex with blue, gives two signals which are signals of complex and rhenium. As

can be seen from these results, it can be concluded that, presence of CO(g) during synthesis is very important and essential in the medium.

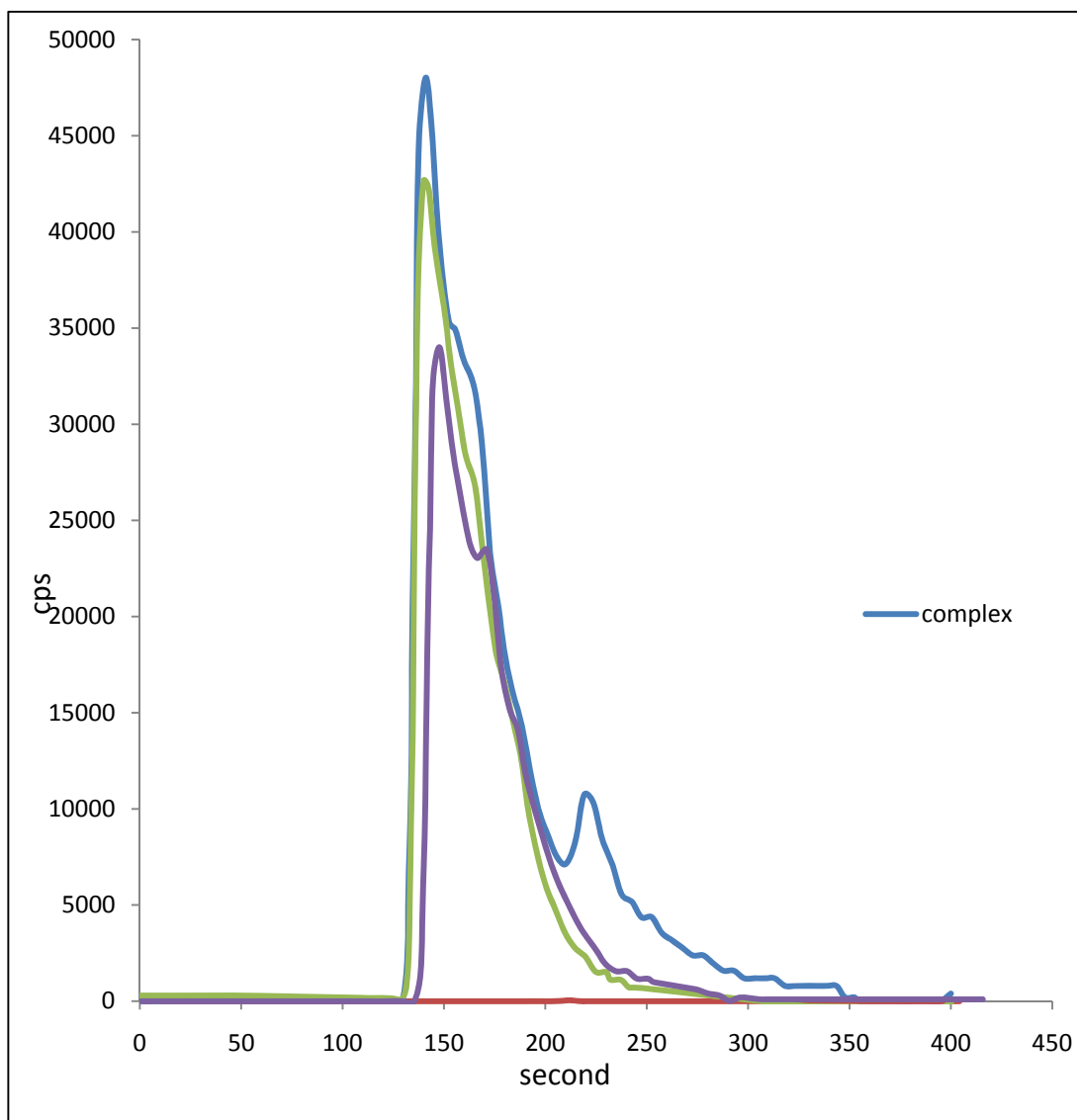


**Figure 44 Optimization studies using Cation Exchange Column**

By comparing the signals in Figure 44, it can be concluded that presence of CO(g) in the medium is important for the formation of carbonyl complex.

When anion exchange column was used, S5 SAX anion exchange column was used as a stationary phase and 5 mM sodium citrate solution in 10.0% MeOH at pH 4.5 was used as the mobile phase with a flow rate of 1.5 mL/min.

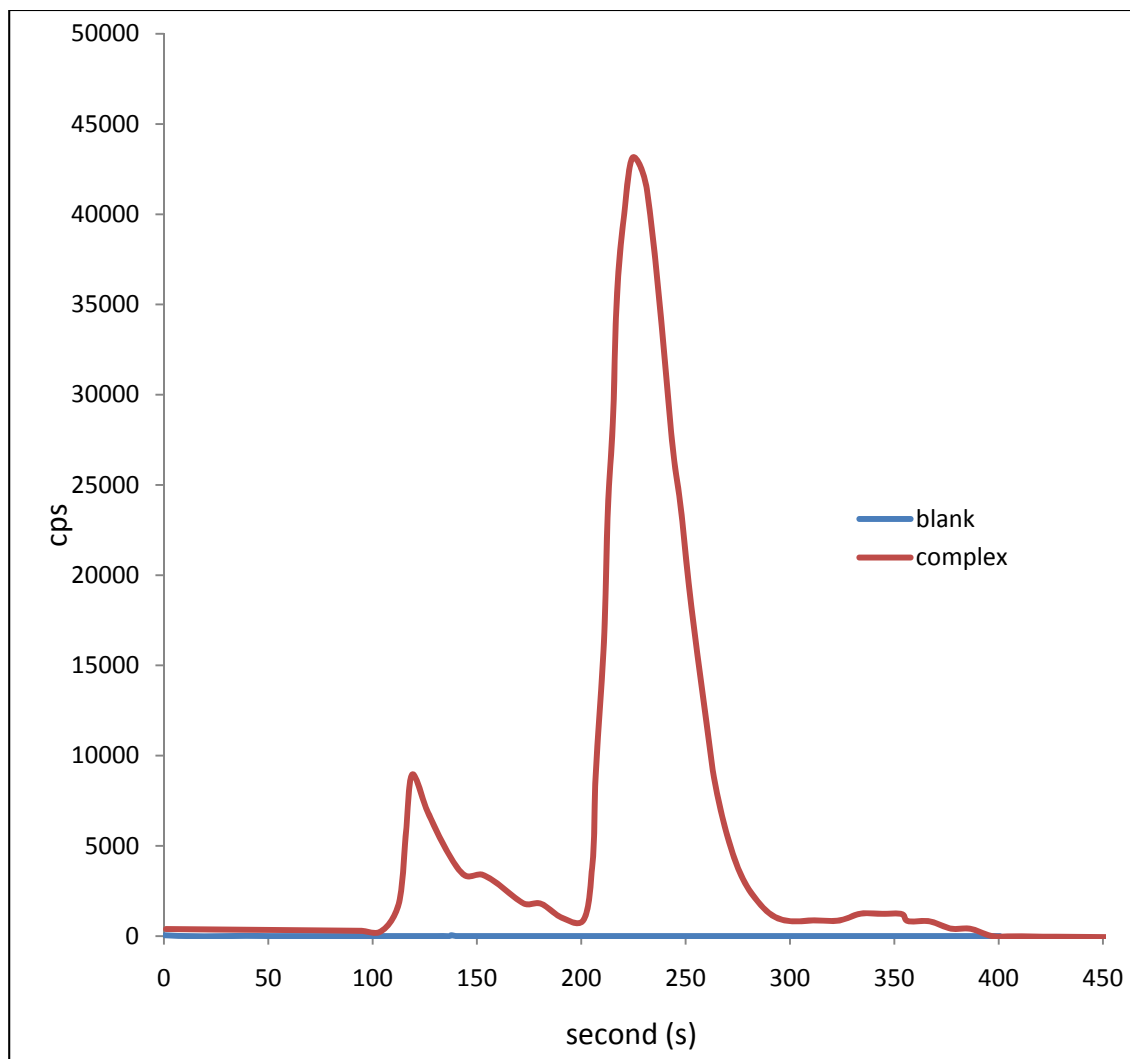


**Figure 45 Optimization studies using Anion Exchange Column**

When Figure 44 is compared with Figure 45, it can be seen that both anion exchange column and cation exchange column gives separation but anion exchange column gives better separation. As it was mentioned before, the complex has a positive charge so in cation exchange column, its signal appears first and in anion exchange column, its signal appear second when compared with the rhenium solution.

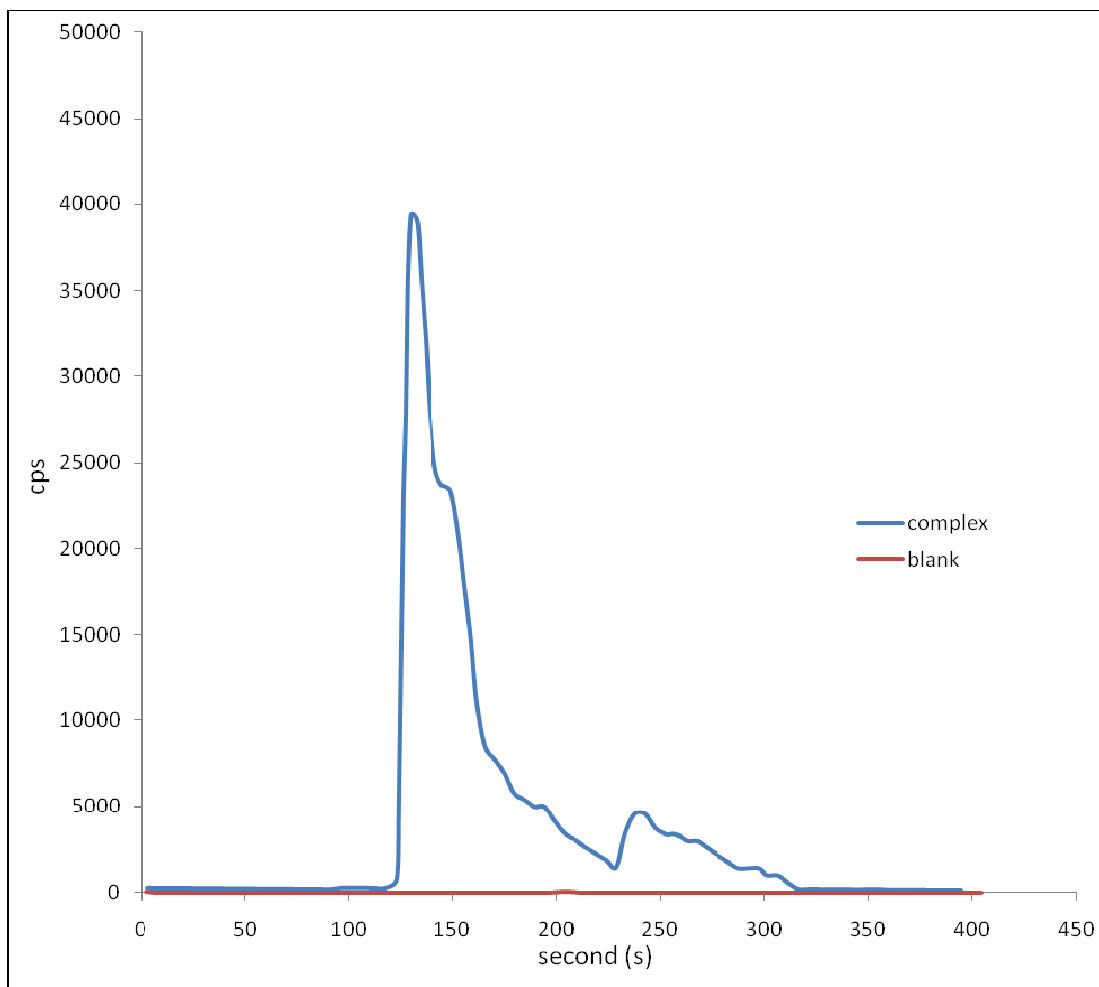


**Figure 46 HPLC-ICP-MS, anion exchange column chromatogram of rhenium carbonyl complex with optimal conditions**

As can be seen from the Figure 46, most of the rhenium was converted into complex. The yield of complex formation is calculated by the ratio of the area of the complex to the total area which are measured by the software of the HPLC instrument. As a result of these calculation, 95 % complex formation is obtained.

Another parameter that is thought to affect complex formation was CO gas flushing. It was observed from optimization studies that 80 minutes is enough for complex formation. At that time, shorter duration times were tried in order to find shorter and suitable duration times in which less CO gas was consumed. The change of the percentage of the complex formation with CO gas flushing time can be seen in Figure

47, as a result of experiment it was concluded that 10 minutes is enough for saturation of  $\text{BH}_3\text{NH}_3$  with CO gas.

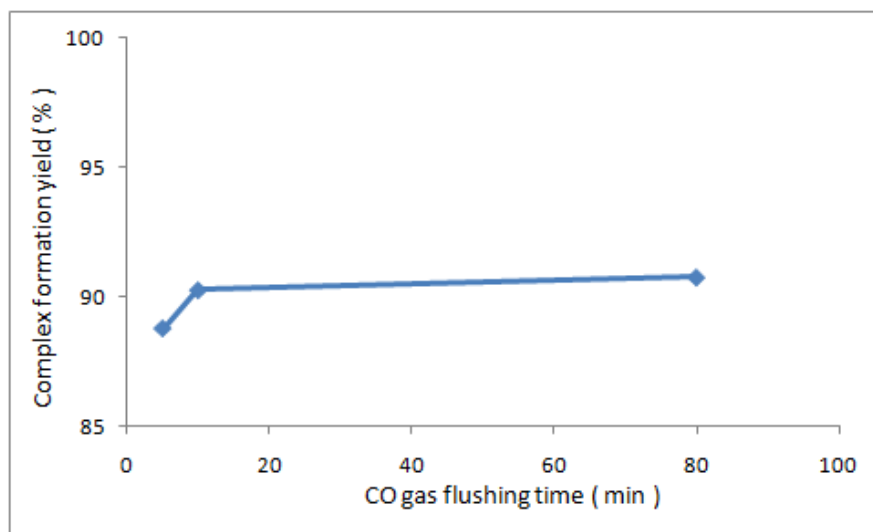


**Figure 47** Complex formation yields at different CO gas flushing times

## CHAPTER 4

### CONCLUSION

Magnetic nanoparticles offer great advantages in biomedicine. Firstly, they are biocompatible and can enter biological units. Second, they are magnetic and they can be controlled by an external magnetic field and lastly they are bioconjugate which enable their interaction with biological units.

Molecular imaging and radiotherapy using radionuclides is gaining popularity in recent years. Magnetic nanoparticles are used in molecular imaging and radiotherapy as they can be controlled by an external magnetic field gradient to magnetically target the particles to the specific sites of the body.

This thesis was a part of an industrial project “The preparation and characterization of silica coated nanoparticles labeled with Tc-99m for magnetically targeted imaging”. This project is performed with the association of METU and Eczacıbaşı- Monrol Nuclear Products. The preparation and characterization of labeled magnetic particles are done by METU. In these studies nonradioactive Rhenium is used as a surrogate of Technetium. In Eczacıbaşı- Monrol Nuclear Product, Technetium is used as an imaging agent. Two different methods were used in the preparation of iron oxide nanoparticles for magnetic targeting. Namely the coprecipitation method and thermal decomposition method.

In this study the thermal decomposition of the iron precursor is used for the preparation of small sized, monodispersed iron oxide nanoparticles.

In thermal decomposition method  $\text{Fe}(\text{acac})_3$  and  $\text{Fe}(\text{CO})_5$  were used as iron source and benzyl ether and phenyl ether were used as solvent. The sizes of the nanoparticles were controlled by changing in the ratio of the concentration of the non coordinating solvent to the concentration of the iron precursors. The average particles sizes of

nanoparticles obtained were all below 10 nm. The size, shape and morphology of nanoparticles were characterized by TEM, XRD and EDX.

In the second part of this study,  $[\text{Re}(\text{CO})_3(\text{OH}_2)_3]^+$  complex was synthesized. Complex is synthesized by reaction of  $\text{NaReO}_4$  with CO gas in an acidic and reducing medium. HPLC-ICP-MS were used for characterization and measurement of complex studies. The 95 % conversion from perrhenate to complex is obtained.

## REFERENCES

- Bean, C., & Jacob, I. (1956). Magnetic Granulometry and Super-Paramagnetism. *Journal of Applied Physics* , 27 (12), 1448-1452.
- Berry, D. A. (2005). Effect of Screening and Adjuvant Therapy on Mortality from Breast Cancer. *The New England Journal of Medicine* 353 , 1784-1792.
- Bronstein, L. M., Huang, X., Retrum, J., Schmucker, A., Pink, M., Stein, B. D., et al. (2007). Influence of Iron Oleate Complex Structure on Iron Oxide Nanoparticle Formation. *Chem. Mater.* , 3624-3632.
- Brown, W. A. (1963). *Micromagnetics*. Interscience.
- Cai, W., & Wan, J. (2007). Facile synthesis of superparamagnetic magnetite nanoparticles in liquid polyols. *Journal of Colloid and Interface Science* 305 , 366-370.
- Cao, J., Wang, Y., Yu, J., Xia, J., Zhang, C., Yin, D., et al. (2004). Preparation and radiolabeling of surface-modified magnetic nanoparticles with rhenium-188 for magnetic targeted radiotherapy. *Journal of Magnetism and Magnetic Materials* 277 , 165-174.
- Caruntu, D., Caruntu, G., Chen, Y., O'Connor, J., Goloverda, G., & Kolesnşchenko, V. L. (2004). Synthesis of Variable-Sized Nanocrystals of Fe<sub>3</sub>O<sub>4</sub> with High Surface Reactivity. *Chem. Mater* 16 , 5527-5534.
- Chouly, C., Pouliquen, D., Lucet, I., Jeune, P., & Pellet, J. (1996). Development of superparamagnetic nanoparticles for MRI: effect of particles size, charge and surface nature on biodistribution. *J. Microencapsul* , 13, 245-55.
- Chunfu, Z., Jinqun, C., Duanzhi, Y., Yongxian, W., Yanlin, F., & Jiajü, T. (2004). Preparation and radiolabeling of human serum albumin (HSA)-coated magnetite nanoparticles for magnetically targeted therapy. *Applied Radiation and Isotopes* 61 , 1255-1259.

- Coey, J. (2010). *Magnetism and Magnetic Materials*. New York: Cambridge University Press.
- Colton, R. (1965). *The Chemistry of Rhenium and Technetium*. London, New York, Sydney: John Wiley & Sons Ltd.
- Dilworth, J. R., & Parrott, S. J. (1998). The biomedical chemistry of technetium and rhenium. *Chemical Society Reviews* , 43-55.
- Gupta, A. K., & Gupta, M. (2005). Synthesis and surface engineering of iron oxide nanoparticles for biomedical applications. *Biomaterials* 26 , 3995-4021.
- Hafeli, U. (2004). Magnetically modulated therapeutic systems. *International Journal of Pharmaceutics* (277), 19-24.
- Hafeli, U. (2004). Magnetically modulated therapeutic systems. *International Journal of Pharmaceutics* 277 , 19-24.
- Hafeli, U., Pauer, G., Failing, S., & Tapolsky, G. (2001). Radiolabeling of magnetic particles with rhenium-188 for cancer therapy. *Journal of Magnetism and Magnetic Materials* 225 , 73-78.
- Hamley, I. (2003). Nanotechnology with soft materials. *Angew Chem Int Ed* 42 , 1692-1712.
- Hamoudeh, M., Salim, H., Barbos, D., Paunoiu, C., & Fessi, H. (2007). Preparation and characterization of radioactive dirhenium decacarbonyl-loaded PLLA nanoparticles for radionuclide intra-tumoral therapy. *European Journal of Pharmaceutics and Biopharmaceutics* 67 , 597-611.
- Hughes, G. (1973). *Radiation Chemistry*. London: Oxford University Press.
- Hyeon, T., Lee, S. S., Park, J., Chung, Y., & Hyon, B. N. (2001). Synthesis of Highly Crystalline and Monodisperse Maghemite Nanocrystallites without a Size-Selection Process. *Journal of American Chemical Society* 123 , 12798-12801.

Jana, N. R., Chen, Y., & Peng, X. (2004). Size- and Shape-Controlled Magnetic (Cr, Mn, Fe, Co, Ni) Oxide Nanocrystals via a Simple and General Approach. *Chem. Mater.* 16 , 3931-3935.

Jana, N. R., Chen, Y., & Peng, X. (2004). Size- and Shape-Controlled Magnetic (Cr, Mn, Fe, Co, Ni) Oxide Nanocrystals via a Simple and General Approach. *Chem. Mater* 16 , 3931-3935.

Jiles, D. (1998). *Introduction to Magnetism and Magnetic Materials*. Florida: Chapman& Hall/CRC.

Jolivet, J. (2000). *Metal Oxide Chemistry and Synthesis: From Solutions to Solid States*. New York: Wiley.

Liang, S., Wang, Y., Yu, J., Zhang, C., Xia, J., & Yin, D. (2007). Surface modified superparamagnetic iron oxide nanoparticles: as a new carrier for bio-magnetically targeted therapy. *J. Mater Sci: Mater Med* 18 , 2297-2302.

Liang, S., Wang, Y., Zhang, C., Liu, Z., Xu, R., & Yin, D. (2006). Synthesis of amino-modified magnetite nanoparticles coated with Hepama-1 and radiolabeled with <sup>188</sup>Re for bio-magnetically targeted radiotherapy. *Journal of Radioanalytical and Nuclear Chemistry* 269 , 3-7.

Lobel, B., Eyal, O., Kariv, N., & Katzir, A. (1999). Temperature Controlled CO<sub>2</sub> laser welding of soft tissues: Urinary bladder welding in different animal models (rats, rabbits, and cats). *Laser Surg Med* (26), 4-12.

Matijevic, E. (1993). *Chem. Mater.* 5 , 412.

Messing, G., Zhang, S., & Jayanthi, G. (1993). *J. Am. Ceram.Soc.* 76 , 2707.

Mozumder, A. (1999). *Fundamentals of Radiation Chemistry*. California: Academic Press.

Myers, H. P. (2002). *Introductory Solid State Physics*. Taylor & Francis.

Pankhurst, Q., Connolly, J., Jones, S., & Dobson, J. (2003). Applications of magnetic nanoparticles in biomedicine. *J. Phys. D: Appl. Phys.* 36 , R167-R181.

Peacock, R. (1966). *The Chemistry of Technetium and Rhenium*. Amsterdam, London, New York: Elsevier Publishing Company.

Pileni, M. (1993). *J. Phys. Chem.* 97 , 6961.

Pratsinis, S., & Vemury, S. (1996). Particle formation in gases- a review. *Powder Technol* (88), 267.

Roca, A. G., Marco, J. F., Morales, M. d., & Serna, C. J. (2007). Effect of Nature and Particle Size on Properties of Uniform Magnetite and Maghemite Nanoparticles. *The Journal Of Physical Chemistry C* , 111, 18577-18584.

Schibli, R., Schwarzbach, R., Alberto, R., Ortner, K., Schmalle, H., Dumas, C., et al. (2002). Steps toward High Specific Activity Labeling of Biomolecules for Therapeutic Application: Preparation of Precursor  $[^{188}\text{Re}(\text{H}_2\text{O})_3(\text{CO})_3]^+$  and Synthesis of Tailor-Made Bifunctional Ligand Systems. *Bioconjugate Chem.* 13 , 750-756.

Simeonidis, K., Mourdikoudis, M. M., Tsiaoussis, I., Martinez-Boubeta, C., Angelakeris, M., Dendrinou-Samara, C., et al. (2007). Controlled synthesis and phase characterization of Fe-based nanoparticles obtained by thermal decomposition. *Journal of Magnetism and Magnetic Materials* 316 , e1-e4.

Spaldin, N. A. (2003). *Magnetic Materials; Fundamentals and Applications*. New York: Cambridge University Press.

Spinks, J., & Woods, R. (1908). *An Introduction to Radiation Chemistry*. United States of America: John Wiley & Sons Inc.

Sun, Y., Duan, L., Guo, Z., Duanmu, Y., Ma, M., Xu, L., et al. (2005). An improved way to prepare superparamagnetic magnetite-silica core shell nanoparticles for possible biological application. *Journal of Magnetism and Magnetic Materials* 285 , 65-70.

Tartaj, P., Morales, M. d., Verdaguier, S. V., Carreno, T. G., & Serna, C. J. (2003). The preparation of magnetic nanoparticles for applications in biomedicine. *J. Phys. D: Appl. Phys.* 36 , R182- R197.

- Teja, A., & Koh, P. (2009). *Prog. Cryst. Growth Charac. of Mater.* 55 , 22.
- Varadan, V. K., Chen, L., & Xie, J. (2008). *Nanomedicine Design and Applications of Magnetic Nanomaterials, Nanosensors and Nanosystems*. West Sussex: John Wiley & Sons Ltd.
- Willard, M., Kurihara, L., Carpenter, E., Calvin, S., & Harris, V. (2004). Chemically prepared magnetic nanoparticles. *International Materials Reviews* , 49 (3-4), 125-163.
- Woo, K., Hong, J., & Ahn, J.-P. (2005). Synthesis and surface modification of hydrophobic magnetite to processible magnetite@silica-propylamine. *Journal of Magnetism and Magnetic Materials* 293 , 177-181.
- Wu, W., He, Q., & Jiang, C. (2008). *Nanosc. Res Lett.* 3 , 397.
- Wunderlich, G., Pinkert, J., Andreeff, M., Stintz, M., Knapp, F., Kropp, J., et al. (2000). Preparation and biodistribution of rhenium-188 labeled albumin microspheres B 20: a promising new agent for radiotherapy. *Applied Radiation and Isotopes* 52 , 63-68.
- Xu, H., Smith, D., & Simon, C. (2004). Strong and bioactive composites containing nano-silica-fused whiskers for bone repair. *Biomaterials* , 25 (19), 4615-26.
- Xu, J., Yang, H., Fu, W., Du, K., Sui, Y., Chen, J., et al. (2007). *Journal of Magnetic Materials* 309 , 307.
- Yih, T., & Wei, C. (2005). Nanomedicine in cancer treatment. *Nanomedicine: Nanotechnology, Biology and Medicine*, 1 , 191-2.